



Observations of vertical mixing in autumn and its effect on the autumn phytoplankton bloom



Juliane U. Wihsgott^{a,b,*}, Jonathan Sharples^a, Joanne E. Hopkins^b, E. Malcolm S. Woodward^c, Tom Hull^{d,e}, Naomi Greenwood^{d,e}, David B. Sivyer^e

^a School of Environmental Sciences, University of Liverpool, Liverpool, UK

^b National Oceanography Centre, Liverpool, UK

^c Plymouth Marine Laboratory, Plymouth, UK

^d Centre for Ocean and Atmospheric Sciences, School of Environmental Sciences, University of East Anglia, Norwich, UK

^e Centre for Environment Fisheries and Aquaculture Science, Lowestoft, UK

ARTICLE INFO

Keywords:

Seasonal cycle
Breakdown of stratification
SML dynamics
Primary production
Autumn phytoplankton bloom
Critical depth
Long-term observations
North-West European Shelf

ABSTRACT

This work examines the seasonal cycle of vertical density structure and its influence on primary production in a temperate shelf sea, with a particular focus on the breakdown of stratification in autumn. We do this by combining new, high resolution observations of water column structure, meteorological forcing, nitrate and chlorophyll fluorescence collected between March 2014 and July 2015 on the North West European Shelf.

Our results challenge the generally accepted assumption that convection dominates over wind driven mixing resulting in seasonal breakdown of stratification. Furthermore we found, that vertical mixing in autumn not only transformed the vertical density structure but also the vertical structure of chlorophyll biomass and surface nutrients. The subsurface chlorophyll maximum was eroded and a vertically homogeneous profile of chlorophyll biomass established itself above the pycnocline. This increased mixing also led to replenishment of surface nitrate concentrations, which supported an autumn phytoplankton bloom. While the significance of phytoplankton blooms in autumn has previously not been well quantified, we argue that these can act as a significant contributor to the seasonal drawdown of carbon.

1. Introduction

Continental shelves are known to be highly energetic and biologically productive regions. Despite only covering ~10% of the ocean surface area, they perform a disproportionately important role within the global carbon cycle (Liu et al., 2010). They support up to a third of all oceanic primary productivity (Wollast, 1998; Bauer et al., 2013), and at least 40 % of oceanic particulate organic carbon (POC) is sequestered on continental margins of depth <200 m (Muller-Karger et al., 2005; Dunne et al., 2007; Regnier et al., 2013). Temperate shelf seas have also been highlighted as being substantial sinks for atmospheric CO₂ (Thomas et al., 2004; Borges et al., 2005; Cai et al., 2006; Cai, 2011).

Away from the influence of fresh river input near the coast, seasonal changes in the vertical water column structure of temperate shelves are dictated by the competition between the stratifying influence of solar irradiance and de-stabilising vertical mixing processes (Simpson and Hunter, 1974; Garrett et al., 1978; Simpson and Bowers, 1984). Tidal

bed stress, wind stress at the surface and convective mixing all make varying contributions to vertical mixing (Pingree et al., 1976; Simpson and Bowers, 1984). The water column structure evolves from one that is fully mixed during the winter months, into a two-layer system during the spring and summer, when the seasonal increase in heat input out-competes the ability of the tides and wind to break down the near surface stratification that additional heating promotes. A loss of heat from the ocean to the atmosphere during the autumn (convection) triggers the breakdown of stratification and a return to fully mixed conditions (Pingree et al., 1976; Townsend et al., 2015). This seasonal cycle of stratification has a significant role to play in determining the light and nutrients available to phytoplankton throughout the year (Gowen et al., 1995; Ji et al., 2008; Sharples et al., 2013; Holt et al., 2014).

The influence the vertical structure has on primary production can be best understood when assessing its constituents and their roles separately. In a simplified two-layer system typical of a summer stratified shelf sea these constituents are the surface mixed layer overlying the

* Corresponding author.

E-mail address: jugott@noc.ac.uk (J.U. Wihsgott).

<https://doi.org/10.1016/j.pocean.2019.01.001>

Received 22 August 2018; Received in revised form 1 December 2018; Accepted 4 January 2019

Available online 08 January 2019

0079-6611/ Crown Copyright © 2019 Published by Elsevier Ltd. This is an open access article under the OGL license

(<http://creativecommons.org/licenses/OGL/3.0/>).

pycnocline region, which itself connects the surface to the bottom mixed layer. The surface mixed layer (SML) is an ubiquitous feature of almost all oceans and describes the topmost layer of the ocean in contact with the atmosphere and is assumed to be fully mixed by wind, wave and/or convective processes. Its variations in depth have strong implications for the exchange of gases, heat and freshwater between the atmosphere and the ocean (e.g. de Boyer Montégut et al., 2004; Belcher et al., 2012; Seguro et al., 2017) but also for biological production (Sharples, 1999; Taylor and Ferrari, 2011; Brody and Lozier, 2014). In fact, the SML constitutes a major control on primary productivity as it impacts on the vertical distribution of phytoplankton and their exposure to nutrients and light (e.g. Sverdrup, 1953; Franks, 2014). The bottom mixed layer (BML) is only found in shallow seas, where tidal mixing is strong enough to homogenise density gradients (Pingree and Griffiths, 1977; Pingree et al., 1982). While the BML is usually nutrient replete it is beyond the euphotic zone. Both the surface and bottom mixed layer are connected by the pycnocline region, which is characterised by the strongest density gradient. Here, the diapycnal transport of momentum, heat and tracers (such as nutrients) between the SML and BML occurs, however this exchange can be restricted by the density gradient within the pycnocline region. Identifying the key processes controlling the vertical density structure is therefore critical to physical and biological oceanography.

The transition from well-mixed to vertically stratified conditions is typically associated with a spring phytoplankton bloom that depletes the nutrient concentrations in the surface, an event that has received considerable attention and one that makes the most important contribution to annual primary production (e.g. Townsend et al., 1994; Rees et al., 1999; Sharples et al., 2006; Liu et al., 2010). During the following summer months, the majority of phytoplankton biomass adapts to survive in low light conditions and becomes concentrated within a sub-surface chlorophyll maximum (SCM) at the base of the pycnocline, in order to take advantage of vertical fluxes of nutrients from bottom waters (Hickman et al., 2012; Williams et al., 2013; Davis et al., 2014). Receiving much less attention in the literature however is the autumnal bloom in phytoplankton, which has been observed in most temperate and subpolar oceans (Longhurst, 1995; Findlay et al., 2006; Behrenfeld, 2010; Song et al., 2010; Martinez et al., 2011).

The classical view suggests that autumn blooms are caused by the deepening of the SML at the end of summer (Findlay et al., 2006; Song et al., 2010). The SML is increased by a combination of shear driven mixing due to wind stress acting on the sea surface during storms for example, and convective overturning of the water column due to cooling of the sea surface. The deepening of the SML subsequently leads to replenishment of nutrients to the euphotic layer by entraining them from below the pycnocline (Pingree et al., 1976; Findlay et al., 2006). For a bloom to occur, light levels need to remain high enough during the deepening to support photosynthesis, despite the increase in SML resulting in phytoplankton receiving less light on average. The deepening of the SML has also been linked to the dilution of grazers, which can further promote phytoplankton growth by decoupling phytoplankton biomass from grazing pressure by zooplankton (Smayda, 1957; Landry and Hassett, 1982; Martinez et al., 2011; Behrenfeld, 2010).

Owing to their small surface signature, short duration and spatial and temporal variability (Colebrook and Robinson, 1961; Hu et al., 2011; Chiswell, 2011; Song et al., 2011), autumn blooms are less well studied than their spring counterparts or the summer SCM, although arguably some of these characteristics can also be attributed to the spring bloom (Thomas et al., 2003; Chiswell, 2011; Song et al., 2011). While observations of the occurrence and strength of autumn blooms have been documented extensively (e.g. Thomas et al., 2003; Aiken et al., 2004; Henson et al., 2009; Chiswell, 2011; Chiswell et al., 2013), its significance within the seasonal cycle of primary production is not well quantified.

In this paper our aim is to investigate the transition of vertical water column structure from summer to autumn, and its effect on the inorganic nutrients and chlorophyll biomass. We do this by combining long-term, high resolution observations of water column structure, inorganic nutrient concentrations, chlorophyll-a fluorescence and meteorological forcing, over the entire seasonal cycle observed in a temperate shelf sea. We will investigate the dominate mechanisms deepening the SML in autumn and estimate their relative contributions. We will further study an autumn phytoplankton bloom that was supported by the deepening of the SML and the subsequent resupply of nutrients to the euphotic layer. Finally, we will estimate the autumn bloom's contribution to the annual primary production of a temperate shelf sea and aim to establish the role the autumn bloom plays within the seasonal cycle.

Improving our understanding of the significance these events play within the seasonal cycle is of fundamental importance to better represent global carbon budgets and predict the response of temperate shelf seas to future climate change.

2. Data collection and processing

In this paper we present new measurements of unprecedented detail spanning 17 months (March 2014 – July 2015), which were collected in a temperate shelf sea on the North-West European Shelf as part of the UK Shelf Sea Biogeochemistry (SSB) programme Sharples et al.. A long-term mooring array in the Celtic Sea collected measurements of full-depth water column structure (Wihsgott et al., 2016) and dynamics, surface inorganic nutrient concentrations, surface chlorophyll-a fluorescence and meteorological forcing. This long-term mooring array consisted of a temperature-salinity logger mooring, a bottom mounted, upward looking acoustic current profiler, a SmartBuoy, maintained by the Centre for Environment, Fisheries and Aquaculture Science (Cefas), and an Ocean Data Acquisition System (ODAS) buoy maintained by the UK Met Office.

In order to get a greater appreciation of the depth variation of biogeochemical variables and to put the autumn bloom event into context, we also incorporate full-depth profiles of CTD, chlorophyll-a fluorescence and inorganic nutrient samples collected during nine process cruises supporting this field campaign. Their names and dates can be found in Table 1.

All observations presented here were taken at the centre of the Celtic Sea (CCS), at a nominal location of 49.4°N and 8.6°W, in a mean water depth of 145.4 m. This location is shown by the white triangle in Fig. 1. The colours in Fig. 1 represent the sea surface temperatures (SST) [°C] during summer 2014. Away from coastal boundaries, warmer SSTs represent seasonally stratified regions and colder SSTs the year-round vertically mixed regions. As can be seen from the relatively warm SSTs surrounding CCS in Fig. 1, the observations were taken in the seasonally stratifying part of the Celtic Sea, well away from any tidal mixing fronts. The site was located centrally on the continental shelf, approximately 120 km northeast of

Table 1
SSB process cruises. Here, DY stands for RRS Discovery and JC for RRS James Cook.

Cruise name	Dates
DY008	18th March – 13th April 2014
JC105	15th June – 24th June 2014
DY026a	03rd August – 15th August 2014
DY026b	15th August – 25th August 2014
DY018	09th November – 03rd December 2014
DY021	01st March – 26th March 2015
DY029	01st April – 30th April 2015
DY030	04th May – 25th May 2015
DY033	11th July – 03rd August 2015

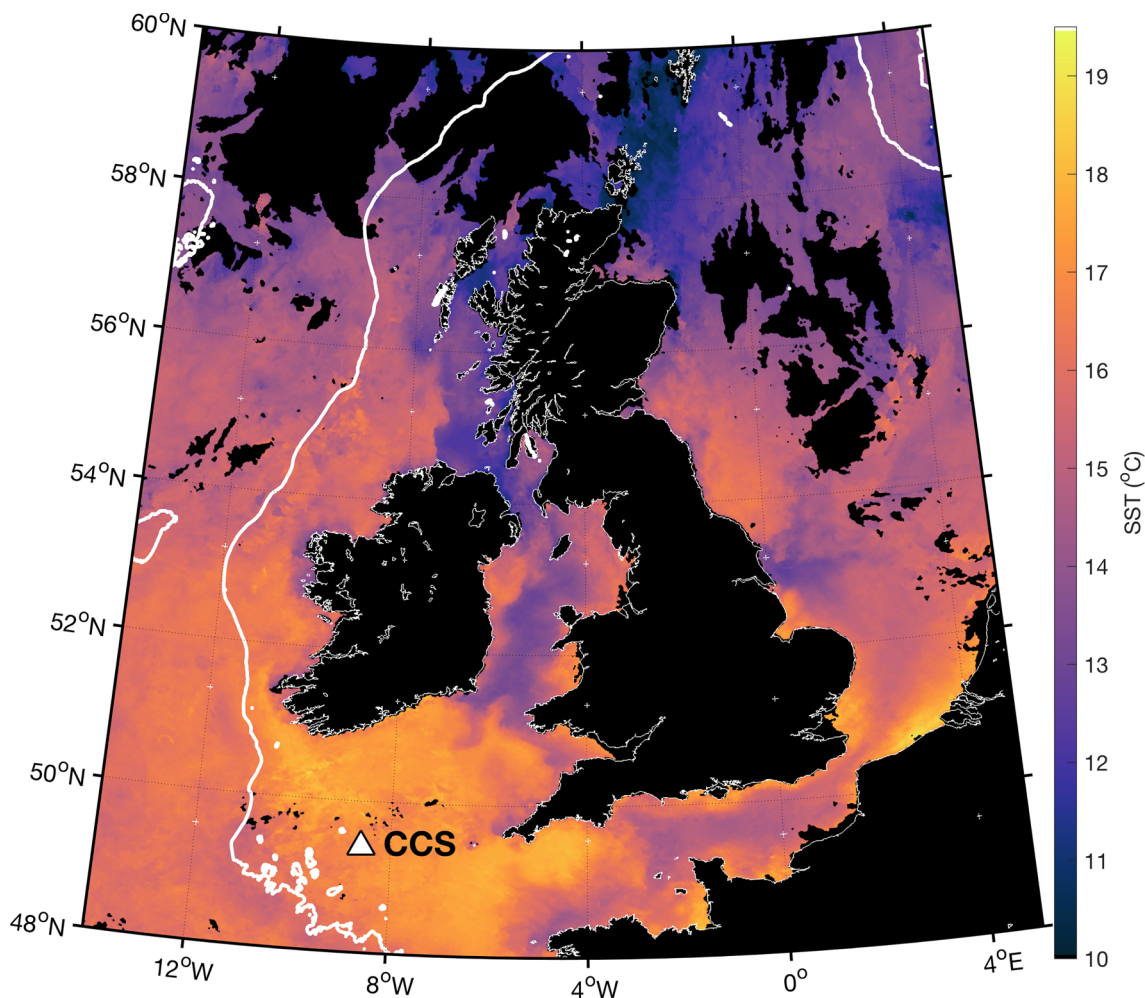


Fig. 1. Sea surface temperature (SST) [°C] around the British Isles during summer 2014. The white triangle marks the location of the central Celtic Sea (CCS) mooring array location. The thick, white line denotes the 200 metre bathymetry contour, which marks the edge of the NW European continental shelf. This satellite image is a 1 week median SST composite, 25th June - 1st July 2014, courtesy of NEODAAS Plymouth Marine Laboratory, UK.

the continental shelf break and approximately 200 km south-west from the British Isles.

2.1. CTD profiles and bottle samples

During each cruise a Seabird 9plus Conductivity-Temperature-Depth (CTD) and a CTG Aquatracka fluorometer mounted on a 24-bottle rosette system collected vertical profiles of temperature, salinity, and chlorophyll-*a* fluorescence (referred to as Chl *a* for the rest of this paper). While Chl *a* is not a direct measure of cell abundance, it is used in this paper as a proxy for chlorophyll biomass.

The raw 24 Hz profiles were extracted, filtered and corrected for thermal inertia using SeaBird data processing Software (Seasave V 7.23.2). The data were subsequently screened and anomalous data removed, averaged onto a 1 db grid and calibrated against samples of Chl *a* concentration and salinity.

Water samples between the surface and near bed were collected on most CTD casts and analysed on board for dissolved inorganic nutrients using a Bran and Luebbe segmented flow colorimetric auto-analyser following classical analytical techniques as described in Woodward and Rees (2001). Our focus in this paper is on nitrate (NO_3) plus nitrite (NO_2), referred to as nitrate hereafter. Clean sampling and handling techniques were employed during the sampling and manipulations within the laboratory, and where possible carried out according to the International GO-SHIP nutrient manual recommendations (Hydes et al., 2010). All samples were analysed as soon as possible after sampling

from the CTD Rosette. Nutrient reference materials (KANSO Japan) were run each day to check analyser performance and to guarantee the quality control of the final reported data. The typical uncertainty of the analytical results was between 2 and 3%, and the limits of detection for nitrate was $0.02 \mu\text{mol l}^{-1}$.

2.2. Mooring observations

The full-depth (10–15 m to sea bed) temperature-salinity (TS) mooring monitored the evolution of the vertical water column structure from March 26th 2014 to July 25th 2015 (Wihsgott et al., 2016). It was designed to capture the vertical structure of the whole water column and had a vertical resolution of 2.5 m in the pycnocline and 5–20 m resolution in the surface and bottom layer. The instruments' temporal sampling resolution was 5 min. After recovery all instruments were calibrated against the ship's CTD data (a SBE 9plus). At each time step, 8 instruments on the mooring took coincident measurements of temperature, conductivity and pressure throughout the water column. To construct full water column profiles of salinity we used a similar method to Hopkins et al. (2014) and fitted a salinity surface as a function of all simultaneous observations of salinity, temperature and time. Delaunay triangulation was then used to evaluate salinity for all available temperature measurements. Potential density, ρ [kg m^{-3}], was derived using the Gibbs-SeaWater (GSW) Oceanographic Toolbox (McDougall and Barker, 2011). To complement the near-surface observations of the TS mooring, we also used temperature data collected

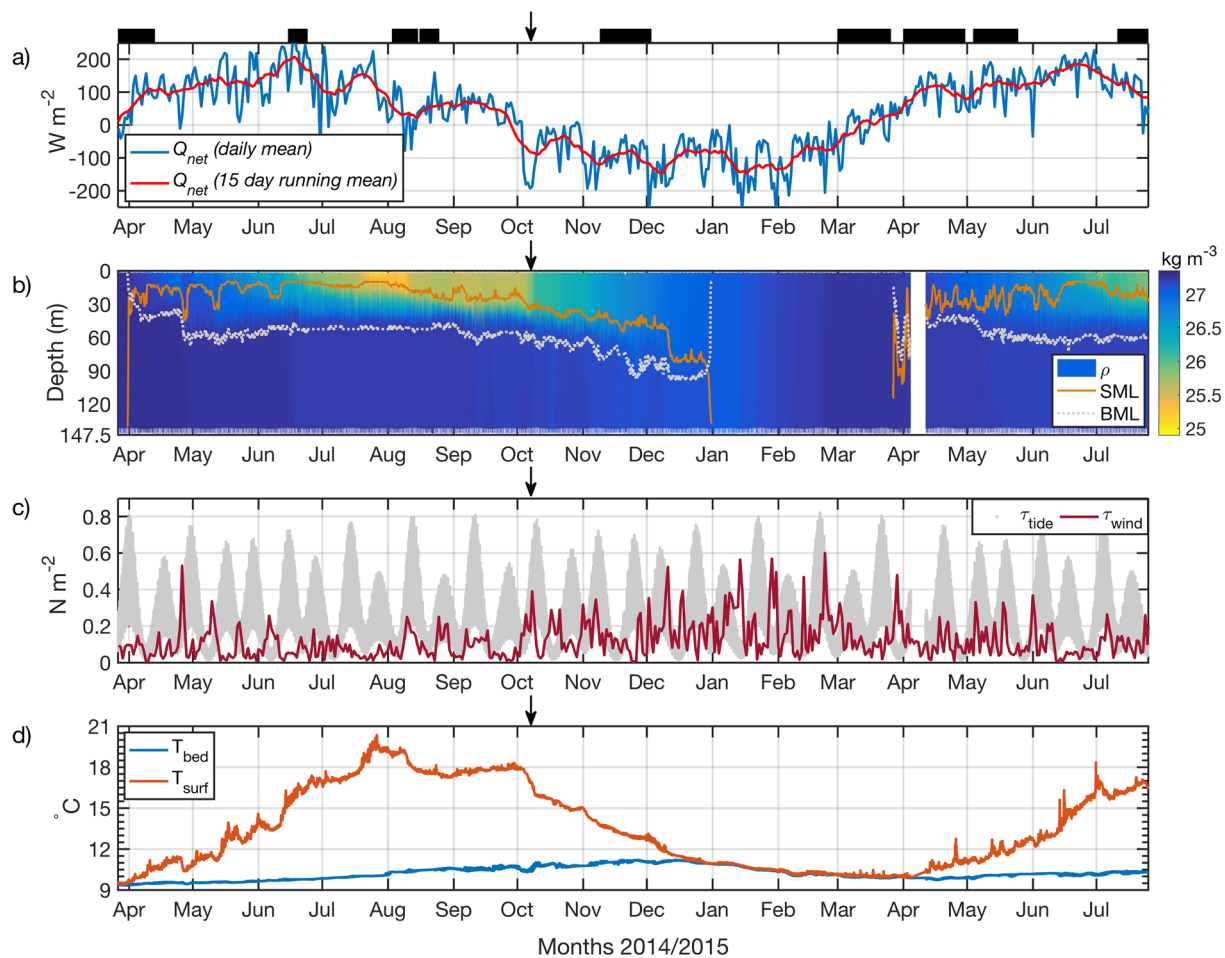


Fig. 2. Physical environment: (a) Q_{net} [$W m^{-2}$] (blue - daily averaged, red - 15 day running average). The black bars above denote the cruise dates (Table 1). (b) full depth observations of ρ [$kg m^{-3}$], overlaid are the SML (solid orange) and BML (dotted grey). (c) daily averages of wind (red) and hourly averages of tidal (grey) stresses [$N m^{-2}$] acting on the sea surface and bed, respectively. (d) Evolution of near bottom (blue) and near surface (red) temperature [$^{\circ}C$]. (For interpretation of the references to colour in this figure legend, the reader is referred to the web version of this article.)

by instruments suspended from a SmartBuoy, maintained by the Centre for Environment, Fisheries and Aquaculture Science (Cefas) and an Ocean Data Acquisition Systems (ODAS) buoy, maintained by the Met Office, at CCS. Over the observational period their setup varied but for the majority of the time, sensors were located between 0.3 and 7.5 m below the sea surface.

A bottom mounted, upward facing 150 kHz FlowQuest acoustic current profiler (ACP) recorded horizontal velocities throughout the whole water column (Wihsgott et al., 2018). The ACP had a vertical resolution of 2 m and a 2.5 min temporal resolution. The current measurements were corrected for time varying magnetic declination, which is the angle between magnetic and true north. Furthermore, the top 14 m of velocity data were removed owing to spurious readings near the sea surface due to side lobe contamination. A battery failure after the 6th May further resulted in loss of data until a new instrument had been deployed on the 9th June 2014.

All TS chain measurements were linearly interpolated onto a $5 \text{ min} \times 2.5 \text{ m}$ resolution grid.

2.2.1. Mixed layer estimates

Mixed layer depth estimates were derived using profiles of potential density collected at the CCS mooring site. Here we define the depth of the surface mixed layer (SML) as a density change of $+0.02 \text{ kg m}^{-3}$ relative to the value at 10 m depth, and the depth of the bottom mixed layer (BML) was defined as a density change of -0.02 kg m^{-3} relative to the value closest to the bed.

2.3. Cefas SmartBuoy

In addition to near surface temperature sensors, the Cefas SmartBuoy sensor package also consisted of a Seapoint Chlorophyll Fluorometer (SCF) [$mg m^{-3}$] and a quantum photosynthetically active radiation (PAR) [$\mu E m^{-2} s^{-1}$] meter (LiCor Inc., USA). The data were stored using the ESM2 data logger, which was configured to sample for 10 min at 1 Hz every 30 min as outlined in Kröger et al. (2009), Hull et al. (2016). In order to correct for instrument drift, the SCF was standardised to arbitrary fluorometry units using fluorescent sulphate microspheres (FluoSpheres, Thermo Fisher Scientific Inc.) after each deployment at the Cefas laboratories. In order to omit artefacts due to non-photochemical quenching, only Chl *a* data that were collected when $PAR < 10 \mu E m^{-2} s^{-1}$ (i.e. hours of darkness) were included in the analysis.

The Cefas SmartBuoy also took measurements of nitrate concentration [$\mu mol l^{-1}$] at the sea surface. Samples were collected using automated water samplers operated by pumping samples into polyethylene bags pre-injected with 5 ml of 1.4 g l^{-1} mercuric chloride ($HgCl_2$ in ultrapure water) as a preservative. On return to shore bag samples were then filtered using $0.2 \mu m$ pore size Whatman Cyclopore polycarbonate filters and analysed using a Skalar SAN plus segmented flow autoanalyser, by standard spectrophotometric methods (Kirkwood, 1996).

2.4. Meteorological observations and heat flux calculations

The hourly observations of wind speed, w [m s^{-1}], relative humidity, h_r [%], air temperature, T_a [$^{\circ}\text{C}$], mean sea level pressure, p [hPa] and air density, ρ_a [kg m^{-3}] recorded by the Met Office ODAS buoy provided the majority of the meteorological data. We complement these observations with shortwave radiation, Q_{sw} [W m^{-2}] and total cloud cover [%] data from the extended-range reanalysis European Reanalysis (ERA)-Interim product of gridded meteorological fields (Dee et al., 2011) from the European Centre for Medium-Range Weather Forecasts (ECMWF). This product integrates observations to model the atmospheric fields across the globe to give 3 hourly datasets with 80 km spatial resolution. The time series used here has been interpolated onto the CCS mooring location. In order to verify the model data, they were compared to observations of the Met Office buoy and the overall fit for the wind speed was found to be good ($R^2 = 0.9097$).

With the combined data the net heat flux, Q_{net} [W m^{-2}] (Fig. 2a), into the ocean was calculated as the sum of all in- and outgoing heat fluxes:

$$Q_{\text{net}} = Q_{\text{sw}} + Q_{\text{lw}} + Q_{\text{sen}} + Q_{\text{lat}}, \quad (1)$$

where Q_{sw} is the shortwave, Q_{lw} is the longwave, Q_{sen} is the sensible and Q_{lat} is the evaporative heat flux. Here, following the convention of the ECMWF fields, all vertical fluxes are defined to be positive downwards. Except for Q_{sw} , which was obtained from the ECMWF reanalysis ERA-Interim product, all other heat fluxes were calculated following Gill (1982).

3. Results

This section will present the high-resolution, long-term observational data introduced above to provide an overview of the physical conditions that prevailed at CCS throughout the 17-month observational campaign of the SSB programme. The length of the observational campaign provided an excellent opportunity to focus particularly on the seasonality, and the chance also to compare recurring events in 2014 and 2015.

3.1. The seasonal cycle at CCS

In general, meteorological conditions intuitively displayed a strong seasonal cycle, most evident in the Q_{sw} (solar irradiance) and thus Q_{net} , which formed a key component of the boundary forcing. The seasonal cycle of Q_{net} , had maxima during June during both 2014 and 2015 and was at a minimum during December - January 2014/2015 (Fig. 2a). Daily averaged Q_{net} reveals the ocean to be gaining heat between the end of March until the end of September 2014 and losing heat from October 2014 to March 2015. This periodicity was less evident in wind speeds, which despite displaying winter maxima were highly variable throughout the observations and provided a constant source of energy with minimum monthly averages of around 7 m s^{-1} during summer 2014 (not shown). Winds were predominantly coming from the southwest. The impacts of meteorological seasonality is clearly evident in the vertical density structure, ρ [kg m^{-3}] provided by the TS mooring at CCS (Fig. 2b) and will be explored in more detail in the following sections.

3.1.1. Onset of stratification in spring 2014

When the TS mooring was first deployed on March 26th 2014, the

water column was still vertically mixed from the previous winter. During the first days of the observations the very top layers of the sea surface stratified during the day with a top-bottom density, ρ , difference of 0.01 kg m^{-3} , however this could not be sustained throughout the diurnal cycle. On March 30th 2014 Q_{net} became predominantly positive (heat gain by the ocean) and supplied more buoyancy than was dissipated by wind and tidal mixing. This marked the onset of spring stratification. In the following days stratification continued to strengthen until April 26th 2014, when a strong low-pressure system passed overhead the mooring site. Wind speeds exceeding 18 m s^{-1} and significant wave heights briefly reaching 9 m (not shown) deepened the SML by 20 m (Fig. 2b). Following the storm, re-stratification of the subsurface layers took place until the water column resembled a typical summer density structure (Fig. 2b). The depth of the SML throughout summer 2014 was on average 20 m. Along with the heat gain at the sea surface through direct heat exchange with the atmosphere, the temperature of the bottom boundary layer also increased by $1.9 \text{ }^{\circ}\text{C}$ between April and December 2014 due to heat transfer through the pycnocline (Fig. 2d).

3.1.2. Breakdown of stratification - convection vs wind forcing during autumn 2014

In October 2014 Q_{net} turned predominantly negative and wind speeds increased compared to the summer months (Fig. 2a & c, average wind speeds of 8.8 m s^{-1} during October - December compared to average wind speeds of 6.75 m s^{-1} during July - September). This led to deepening of the SML depth and marked the beginning of the breakdown of stratification in 2014 (arrows in Fig. 2). During this period negative heat fluxes rarely occurred in isolation from strong wind forcing at CCS. In order to determine whether the breakdown of stratification was driven by shear driven processes caused by wind stress or convective mixing due to buoyancy reduction initiated by negative heat fluxes, the Obukhov length scale, L_{OB} [m] (Obukhov, 1946) was used to examine this competition:

$$L_{\text{OB}} = -\frac{u_*^3}{\kappa B_0} \quad (2)$$

Here, u_* [m s^{-1}] is the friction velocity, $u_* = \left(\frac{\tau}{\rho_0}\right)^{1/2}$, where τ [N m^{-2}] is the wind stress, and $\rho_0 = 1026 \text{ kg m}^{-3}$ is the reference density. $\kappa = 0.41$ is the von Kármán constant, and B_0 [$\text{m}^2 \text{ s}^{-3}$] is the surface buoyancy flux. Considering that temperature is the dominant control on density in the Celtic Sea (Pingree et al., 1976; Simpson and Hunter, 1974) we estimate B_0 to be directly proportional to Q_{net} using $B_0 = \frac{\alpha g}{c_p \rho_0} Q_{\text{net}}$. Here, α [$^{\circ}\text{C}^{-1}$] is the thermal expansion coefficient of seawater calculated using the GSW Oceanographic Toolbox (McDougall and Barker, 2011), $g = 9.81 \text{ m s}^{-2}$ is the acceleration due to gravity and $c_p = 3985 \text{ J kg}^{-1} \text{ }^{\circ}\text{C}^{-1}$ is the heat capacity of seawater. Similar to the observed and calculated heat flux terms introduced earlier, B_0 was defined to be positive downwards.

The $|L_{\text{OB}}|$ specifies the vertical extent over which either convection or mechanical stirring (at the boundary) is the dominant surface mixing mechanism (Taylor and Ferrari, 2011). If the water column is unstable due to strong surface cooling (negative Q_{net}) the L_{OB} is greater than 0 ($L_{\text{OB}} > 0$). In contrast, if the water column is vertically stratified due to positive heat fluxes the L_{OB} is less than 0 ($L_{\text{OB}} < 0$). Coupling the Obukhov length scale with the depth of the surface mixed layer, Brody and Lozier (2014) define three surface regimes controlling the SML (Table 2) that we use here to help identify the contribution that

Table 2
Surface regimes controlling the SML.

Convective mixing regime case 1	$ L_{\text{OB}} < \text{SML}$ while $B_0 < 0$ and hence $Q_{\text{net}} < 0$
Wind mixing regime case 2	$ L_{\text{OB}} > \text{SML}$
Heat regime case 3 (stratification counteracts mixing)	$ L_{\text{OB}} < \text{SML}$ while $B_0 > 0$ and hence $Q_{\text{net}} > 0$

convection and wind-mixing make to autumnal deepening of the SML. When the buoyancy flux is large and negative (the ocean is losing heat to the atmosphere), and wind speeds are low, convection is the dominant control on the SML depth (case 1, Table 2). In contrast, when wind speeds are moderate to large, the wind becomes the driver of surface mixing and SML deepening (case 2, Table 2). The sign of the Q_{net} and thus B_0 are irrelevant on this occasion. In case of a small positive net heat/buoyancy flux, which promotes stable stratification ($L_{OB} < 0$), the wind becomes the sole surface mixing mechanism by default. When the buoyancy flux is large and positive, stratification counteracts any surface mixing and SML deepening is suppressed (case 3, Table 2).

Using hourly data of observed wind speed, w , and net heat flux, Q_{net} , the L_{OB} was calculated for the entire time series. These hourly results of the L_{OB} were then compared to the SML (Fig. 2b) and categorised accordingly for each day, using the criteria in Table 2. Subsequently, a relative contribution was attributed to each regime on a daily basis, e.g. if $|L_{OB}| > SML$ for 12 h during the 10th October 2014, then wind forcing was considered the dominant SML affecting mechanism during 50% of that day. To filter out some of the short term variability owing to sporadic events in heating and wind forcing, the daily contributions were smoothed using an 8 day running average (Fig. 3a).

As might be expected from the observed Q_{net} (Fig. 2a), the convective and heating regime (cases 1 & 3 Table 2) displayed a clear seasonal cycle (Fig. 3a), with convection more dominant during winter, and heating in the summer months. While the wind regime (case 2

Table 2), was less seasonal, it dominated throughout the observational campaign (53% of the entire observational period). During the period of the active SML deepening (2nd October - 31st December 2014, grey bar Fig. 3a), the contribution of both wind and convection (cases 1 & 2 Table 2) increased compared to the rest of the year, and the heating regime (case 3 Table 2) was completely shut off at times. Despite several periods of sustained surface cooling occurring during autumn 2014 (Fig. 2a), the wind regime significantly increased its control on the SML (two sample t -test: $p < 0.01$, t -test), being dominant 63% of the time the SML deepened (2nd October - 31st December 2014). Periods when the convective regime was dominant accounted for 32% of this time, which coincided with low wind speeds/stresses (Fig. 3b-c). This represents a statistically significant increase of 8% (two sample t -test: $p < 0.01$) compared to the whole observational period. Periods when positive stratification counteracted wind mixing (case 3 Table 2) accounted for the least amount of time during the SML deepening period, of 5%. While shear stresses due to wind appear to be the dominant SML deepening mechanism, considerable variability between and within days was observed. Fig. 3b-d demonstrate this short-term variability by focusing on a 2 week period in December 2014. The main sources of this variability was the diurnal heat cycle and the relatively short duration of some wind events.

This is an interesting and potentially significant result as it challenges many previous assumptions that convection is the dominant mechanism driving seasonal breakdown of stratification in shelf seas

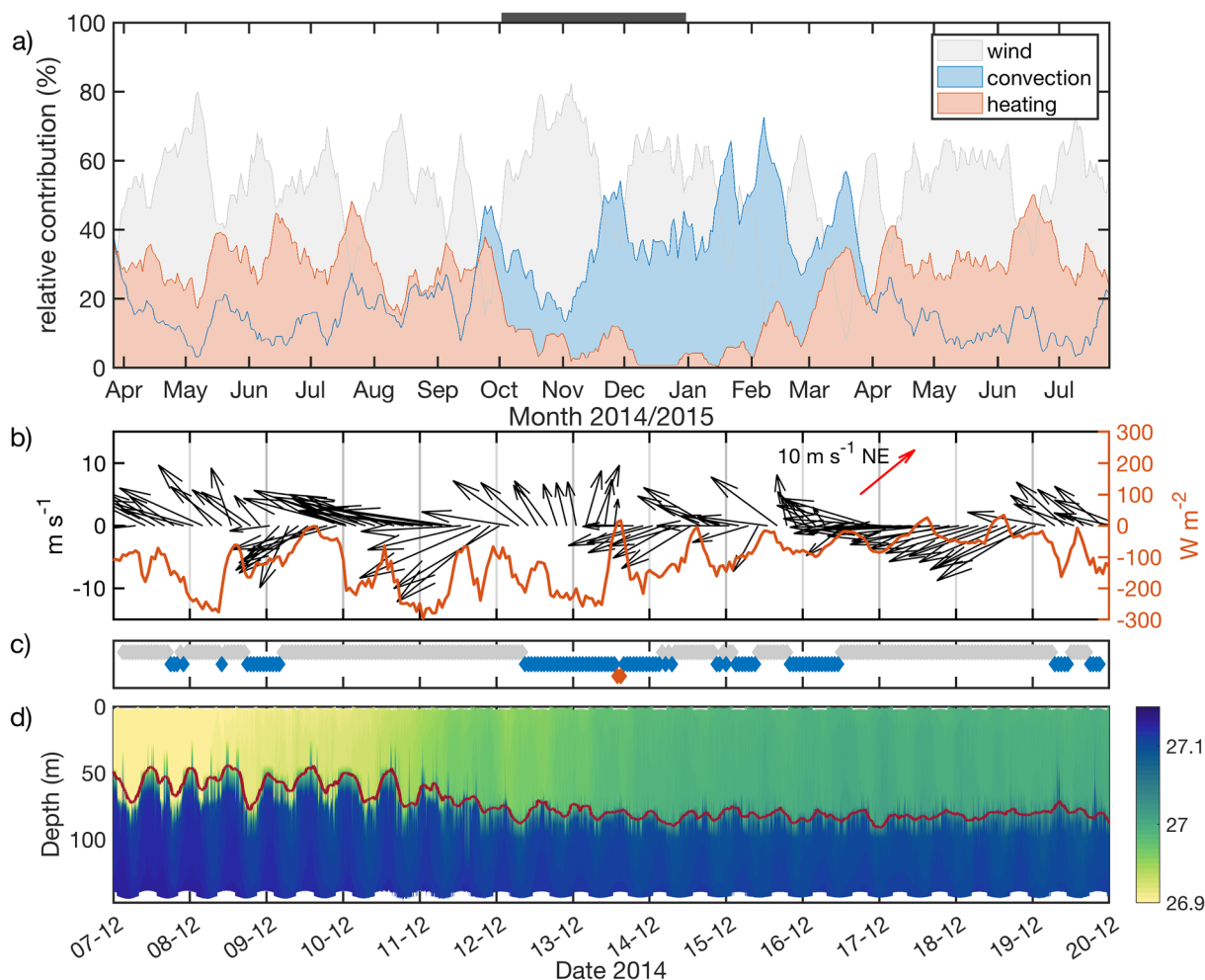


Fig. 3. Dominant controls on SML: (a) 8 day running average of proportional control on SML: wind (grey), convective (blue) and heat (red) regime. The grey bar above marks the SML deepening period, October 2nd - December 31st 2014. (b) Observed w [$m s^{-1}$] and wind direction (black) and Q_{net} [$W m^{-2}$] (orange) (c) Dominant surface regimes controlling the SML: wind (grey), convective (blue) and heat (red) (d) Observed ρ [$kg m^{-3}$] with overlaid SML depth [m] (red) during a 2 week period in December 2014. (For interpretation of the references to colour in this figure legend, the reader is referred to the web version of this article.)

(Edinger et al., 1968; Nielsen and St. John, 2001; Townsend et al., 2010), as well as in open-ocean environments, (Kraus and Turner, 1967; Lacombe et al., 1970; Marshall and Schott, 1999; Taylor and Ferrari, 2011). While an attempt has been made to separate the individual contributions from wind and convection, the observed mixing effects on the density structure are difficult to distinguish as they both contribute to the same process of deepening the SML. We note that the dependence of both the sensible and the latent heat flux (Q_{sen} , Q_{lat}) on the wind speed, w , ensures that the sum of all heat fluxes, Q_{net} , can never act fully decoupled from the wind forcing. Furthermore, both convection and shear driven mixing can aid each other to be more efficient at deepening the SML. Convection can act to better connect surface mixing processes with the stratified interior by homogenising the surface boundary layer, supporting further breakdown of seasonal stratification. Whereas wind stress can aid convection by disrupting the thin viscous sublayer and thereby permitting a more rapid transfer of heat through the sea surface.

During the winter months of January and February 2015 the water column was further losing heat to the overlying atmosphere and eventually cooling down to approximately 10°C (Fig. 2d). While the water column was vertically fully mixed for most of the winter months, periods of transient stratification did exist. These generally only lasted one day but could occur for up to 5 consecutive days but the stratification only manifested itself in the top 10 m of the water column.

On March 26th 2015 the buoyancy input of the positive heat flux became strong enough to overcome the wind and tidal mixing and the water column began to re-stratify. While the timing of the onset of stratification is similar to 2014, the rate at which stratification was strengthening was lower during 2015. This resulted in the water column being less strongly stratified at any time during 2015 compared to the previous year (Fig. 2d, Fig. 4a). At the end of the observational period in July 2015 the difference in top-bottom density difference was 0.75 kg m⁻³ less than observed in July 2014 (Fig. 4a).

In summary, the observed evolution of water column structure was typical for a seasonally stratifying shelf sea, such as the Celtic Sea. Here, the change in vertical water column structure is predominantly a vertical exchange process driven by the competition of buoyancy input versus stirring at the boundaries i.e. sea surface/bed (Simpson and Hunter, 1974; Garrett et al., 1978; Simpson and Bowers, 1984). The buoyancy input was supplied by Q_{net} at the sea surface, whereas wind and tides were supplying stirring powers to mix gradients near the sea surface and sea bed.

3.2. Seasonal cycle of chlorophyll-*a* and inorganic nitrate concentrations

The seasonal cycle of primary production in the Celtic Sea is, like in other seasonally stratifying shelf sea regions, tightly coupled to the change in vertical water column structure (Tett et al., 1993; Thomas et al., 2003; Hu et al., 2011; Sharples et al., 2013). The long-term observations of surface Chl *a* and nitrate shown in Fig. 4c and d demonstrate a clear response to the physical events described above. At the end of winter in March 2014, before stratification was fully established (Fig. 4a), Chl *a* concentrations were low ($< 1 \text{ mg m}^{-3}$) and nitrate concentrations were high ($\sim 9 \mu\text{mol l}^{-1}$) throughout the water column. As spring stratification became established a spring phytoplankton bloom was initiated, which peaked on April 11th 2014 with surface Chl *a* concentrations of up to 6.2 mg m⁻³. Consequently the available nitrate in the surface mixed layer (SML) became quickly depleted and concentrations dropped to $\sim 2.5 \mu\text{mol l}^{-1}$. During the following summertime stratified period, the diapycnal transport of momentum, heat and tracers was restricted due to suppressed turbulent motions at the pycnocline. Thus the resupply of inorganic nutrients from the dark, nutrient rich bottom waters to the well-lit, nutrient depleted surface waters was inhibited. The resulting nutrient limitation, and potentially also an increased impact of grazers, led to a decrease in the surface population and the demise of the spring phytoplankton bloom. The

secondary peak in surface nitrate concentration around April 26th 2014 was induced by a strong storm event described above. Here, strong wind and waves deepened the SML by 20 m (Fig. 2b) and thereby entrained dissolved nutrients from the BML, raising surface nitrate concentrations to 6.9 $\mu\text{mol l}^{-1}$. Subsequently a secondary phytoplankton bloom was initiated, with surface Chl *a* concentrations of up to 9 mg m⁻³ that peaked on May 4th 2014.

On May 12th the SmartBuoy platform drifted away from its location and hence no surface nitrate and Chl *a* observations were available from CCS until June 19th 2014. At this time the vertical profiles of density, nitrate and Chl *a* resembled that of a typical shelf sea summer profile as also observed in other shelf seas e.g. (Williams et al., 2013; Townsend et al., 2015; Du et al., 2017). Compared to the spring phytoplankton bloom at the surface, the biomass peak had been shifted to the interior of the water column to the SCM. In all coincident, full depth profiles of CTD, nitrate and Chl *a* at CCS, the SCM was located within the base of the pycnocline and in the vicinity of the nitracline. Here, turbulence from tidal and internal mixing mechanisms, for example internal waves, together with the strong nutrient gradient (the nitracline) caused an upward flux of nutrients that sustained this biomass peak (Williams et al., 2013; Lee et al., 2016; Du et al., 2017). Peak concentrations of Chl *a* within the SCM were variable (average $2.06 \pm 0.92 \text{ mg Chl } a \text{ m}^{-3}$; $n = 9$), while Chl *a* concentrations within the SML were uniformly low (average $0.31 \pm 0.1 \text{ mg Chl } a \text{ m}^{-3}$; $n = 9$).

The breakdown of stratification commenced in early October 2014 due to increased wind mixing and, to a lesser extent, also surface cooling (Fig. 3a). While this resulted in a deepening of the SML and sharpening of the pycnocline (Fig. 3c), it also transformed the vertical structure of chlorophyll biomass and inorganic nutrients. Fig. 5 illustrates the change in vertical structure between summer (Fig. 5a-c) and autumn (Fig. 5d-f): The deepening of the mixed layer resulted in entrainment of nutrients from below the pycnocline, which increased surface nitrate concentrations by $2.1 \pm 0.1 \mu\text{mol l}^{-1}$ (Fig. 4d). This increase is seen over the entire SML (Fig. 5b & e). The deepening also led to the erosion of the SCM and a vertically homogenous profile of chlorophyll biomass was established above the pycnocline (Fig. 5c & f). Simultaneously we observed an increase in surface Chl *a* concentrations of up to 2.2 mg m⁻³ (Fig. 4c), which could be indicative of an autumn phytoplankton bloom driven by the resupply of nutrients replenished by SML deepening. Surface light levels were low during this period, and less than half of spring and summer PAR levels (Fig. 4b).

Surface Chl *a* concentrations dropped to winter background levels of $< 1 \text{ mg m}^{-3}$ around December 13th 2014 and stayed low during the mixed period. While nitrate data were unusable between October 16th 2014 and March 20th 2015 due to problems with the preservative, pre bloom nitrate concentrations of $\sim 7.5 \mu\text{mol l}^{-1}$ were observed during the DY021 February process cruise.

The phytoplankton spring bloom that followed the onset of stratification in 2015, was significantly stronger in magnitude compared to 2014, with peak surface Chl *a* concentrations of up to 11 mg m⁻³ (Fig. 4c). In general, the 2015 bloom had several peaks and hence the main bloom event was less well defined compared to 2014. Following the bloom Chl *a* concentrations within the SML, surface values dropped back to low summer values (average $0.16 \pm 0.05 \text{ mg Chl } a \text{ m}^{-3}$; $n = 40$). Peak Chl *a* concentrations within the SCM in the following summer were again variable (average $1.05 \pm 0.41 \text{ mg Chl } a \text{ m}^{-3}$; $n = 40$).

4. Discussion

We have presented observations of the evolution of vertical water column structure throughout the seasonal cycle of 2014 and 2015, and showed a clear response of Chl *a* and nitrate to these events. We find that the deepening of the SML depth in autumn 2014, which was mostly driven by wind mixing, replenished inorganic nutrient concentrations in the surface layer. Simultaneously, we observed the erosion of the

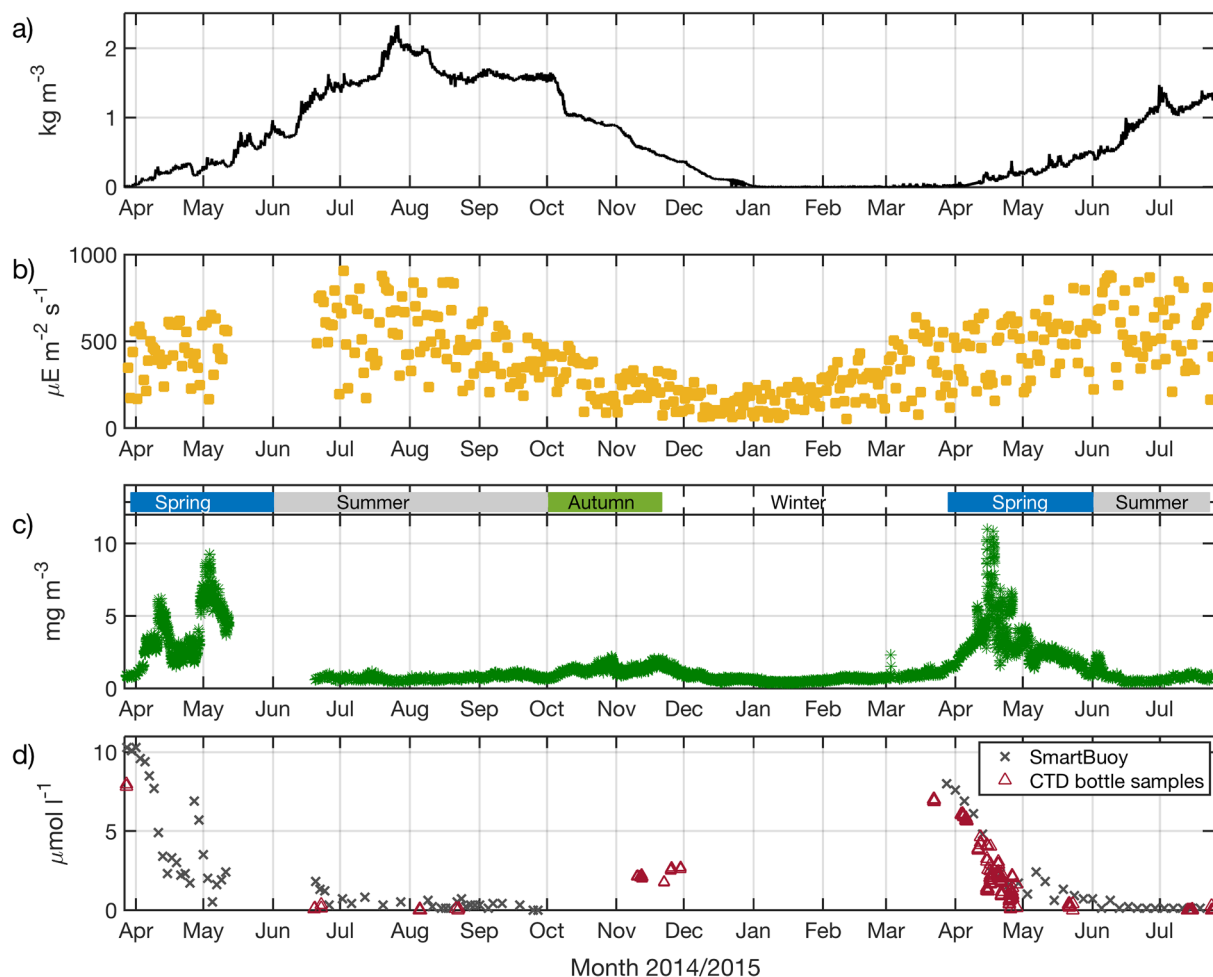


Fig. 4. Combined physical and biogeochemical observations: (a) top-bottom ρ difference [kg m^{-3}]. (b) daily averaged PAR [$\mu\text{E m}^{-2} \text{s}^{-1}$]. (c) surface Chl a [mg m^{-3}]. The bars above mark the duration of each seasonal regime. (d) surface nitrate concentration [$\mu\text{mol l}^{-1}$].

summer SCM peak by homogenising the vertical chlorophyll biomass profile over the entire SML. We will now consider whether the observed increase in Chl a during the autumn is linked to in situ phytoplankton growth as a result of replenishment of nutrients, or simply a redistribution of the subsurface phytoplankton community. We will also examine the role that light availability plays in terminating the autumn bloom. Finally, using the well resolved time series of water column structure and changes in nutrient concentrations throughout the year, we make an estimate of the contribution to new production, i.e. the proportion of primary production that is supported by nitrate (Dugdale and Goering, 1967), made by the autumn bloom and compare this to estimated and measured rates of productivity during the spring and summer months.

4.1. In-situ growth in autumn

The depth integrated Chl a biomass can be used to help determine whether a phytoplankton population is actively growing in response to additional resource availability (light or nutrients), or whether changes in Chl a concentration are simply redistributed due to vertical mixing of the water column. Fig. 6 shows the seasonal cycle of depth integrated chlorophyll biomass during the stratified periods of 2014 and 2015. For each CTD cast at CCS this was calculated by taking the depth integral from the surface to the top of the BML. In most vertical profiles of Chl a we found evidence of photochemical quenching during daytime CTDs in the near surface. To avoid underestimating the depth integrated chlorophyll biomass we extrapolated Chl a values from the SML depth

to the near surface using nearest neighbour extrapolation for all daytime CTDs. This led to an average increase of 4% compared to using non-corrected profiles of Chl a .

In order to estimate depth integrated biomass from surface Chl a concentrations, recorded by the SmartBuoy, we assumed a homogeneous profile of Chl a throughout the SML as observed during DY018 (Fig. 5f). We then calculated the depth integral from the surface to the SML depth, and hence this should be considered as a minimum estimate of chlorophyll biomass.

As might be expected, the highest observed values of up to 186 mg m^{-2} were found during the spring bloom cruise (DY029) in 2015. In contrast to this, the summer values (JC105, DY026a/b, DY030 and DY033) were relatively low, yet variable (average $21.33 \pm 9.89 \text{ mg Chl } a \text{ m}^{-2}$, $n = 55$), but similar in magnitude to values observed by Hickman et al. (2012) in the Celtic Sea. As soon as the vertical water column structure began to break down in early October 2014, we observed a sharp increase in integrated chlorophyll biomass of up to 90 mg m^{-2} compared to summer values (Fig. 6). This increase is indicative of in situ growth fuelled by the resupply of inorganic nutrients to the euphotic layer from depth, as opposed to redistribution of Chl a , and the availability of sufficient light to sustain an autumnal phytoplankton bloom. Evidence of enhanced primary production during DY018 indicative of an autumn phytoplankton bloom was also found in other studies: García-Martín et al. (2017) found evidence that the system at CCS turned net-autotrophic during DY018 thus acting as a sink of CO_2 due to primary production. Giering et al. (2018) observed a secondary peak in the abundance of nauplii and copepodites

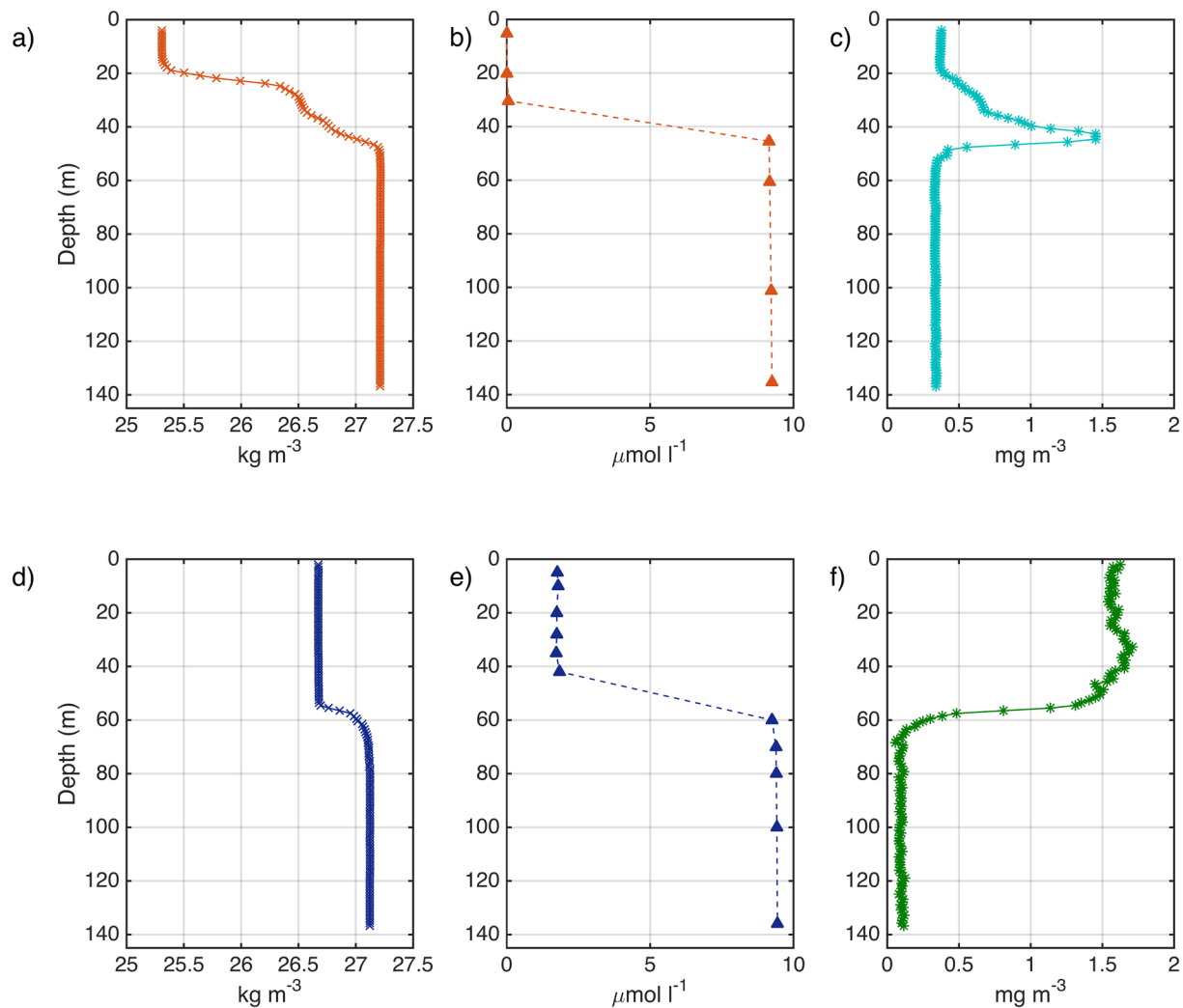


Fig. 5. Vertical profiles during (a)–(c): summer (DY026a/b) and (d)–(f): autumn (DY018). (a) & (d) potential density [kg m^{-3}]. (b) & (e) nitrate [$\mu\text{mol l}^{-1}$]. (c) & (f) Chl α [mg m^{-3}].

(zooplankton), indicative of an autumn phytoplankton bloom. Further evidence was also observed by Davis et al. (2018), who noted increases of particulate organic carbon (POC) and particulate organic nitrogen (PON) during DY018, similar to the signal they observed during the spring phytoplankton bloom in 2015 (DY033).

4.2. Light limitation during autumn

As mentioned earlier the in situ light levels during the autumn period were less than half compared to those experienced during the spring and summer months (Fig. 4b), yet clearly sufficient for the onset of the autumn phytoplankton bloom (Fig. 4c, Fig. 6). Despite this a change in phytoplankton production must have occurred, as we noticed the presence of significant levels of nitrate concentrations of $2.1 \mu\text{mol l}^{-1}$ on average throughout the SML during DY018 (Fig. 4d, Fig. 5e). While biomass was increasing, phytoplankton did not deplete the newly available nitrate pool to undetectable levels, which is normally the case during spring and summer conditions (Fig. 4c and d) when surface phytoplankton communities are thought to be nitrogen (N) limited in the Celtic Sea (Pemberton et al., 2004; Davis et al., 2014; Williams et al., 2013). The presence of nitrate within the SML during autumn is thus an indication that primary production within the SML had shifted from N-limited production during spring and summer to light limited production, which was also suggested by Poulton et al. (2017) based on their observed phytoplankton turnover times.

We want to further study this light limitation by comparing the SML depth to the critical depth, z_{cr} , the theoretical depth at which vertically integrated phytoplankton growth outweighs losses. The concept of z_{cr} was developed by Sverdrup in 1953 as part of his critical depth theory (SCD) (Sverdrup, 1953), which predicts the onset of a phytoplankton bloom when the actively turbulent layer shoals above the critical depth (Franks, 2014). As a result phytoplankton are no longer light limited, growth outweighs losses, and a bloom can occur. This concept has been usually applied to study the mechanisms triggering the onset of the spring phytoplankton bloom (Siegel et al., 2002) but has recently received considerable debate regarding its validity (Behrenfeld, 2010; Taylor and Ferrari, 2011; Brody and Lozier, 2014). Interestingly, Chiswell (2011) & Chiswell et al. (2015) proposed that the SCD may actually apply in autumn and winter to determine the shut-off of primary production. One of the SCD's main assumption regards an actively turbulent surface layer that ensures equal light exposure, rather than a surface mixed layer that is defined by a fixed difference in temperature/density to a near surface value (Franks, 2014). In contrast to most spring conditions, during autumn the SML is approximately equal to the actively turbulent layer, as the SML is being actively deepened, which homogenises the surface layer (Fig. 5d–f). We therefore use the SML depth as an indicator for the depth of the turbulent layer during autumn. Values for z_{cr} were calculated using

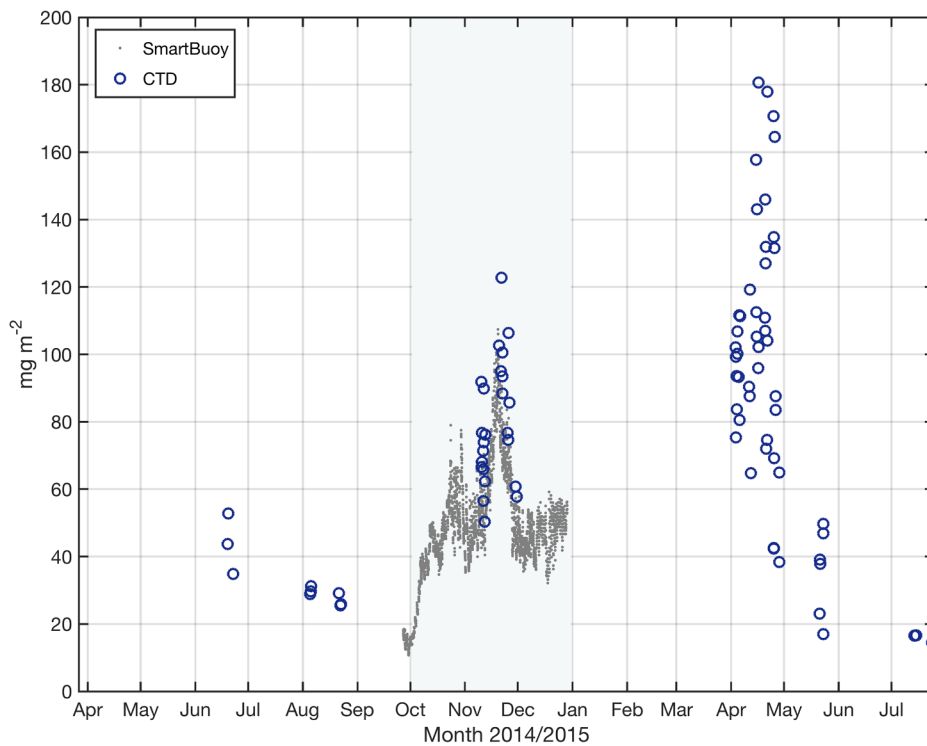


Fig. 6. Depth integrated Chl *a* biomass [mg m^{-2}]. Markers denote the SmartBuoy platform and CTD derived values during the stratified periods of observations. The shaded area denotes the time of active SML deepening (October 2nd - December 31st 2014). For comparison we also included SmartBuoy data before the breakdown of stratification started.

$$\frac{1}{Kz_{cr}}(1 - e^{-Kz_{cr}}) = \frac{I_c}{I_0} \quad (3)$$

where $K = 0.1 \text{ m}^{-1}$ is the attenuation coefficient, I_c [$\text{mol m}^{-2} \text{ d}^{-1}$] is the compensation irradiance, where integrated losses and production balances, and I_0 [$\text{mol m}^{-2} \text{ d}^{-1}$] is the surface irradiance. Here, we calculated z_{cr} for $I_c = 1.24 \text{ mol m}^{-2} \text{ d}^{-1}$ a value obtained by Siegel et al. (2002) for an open ocean zonal average between 45 and 50° N, and $I_c = 3.03 \text{ mol m}^{-2} \text{ d}^{-1}$ a value observed by Langdon (1988) for a coastal dinoflagellate. We also compare these to z_{cr} values calculated for the Celtic Sea by Pingree et al. (1976).

As might be expected, all variants of z_{cr} show a clear seasonal cycle with deepest values during summer and shallowest during winter (Fig. 7a), which is in good agreement with the magnitude of surface irradiance (Fig. 4b). While the values calculated by Pingree et al. (1976) clearly show a stronger response to the seasonal cycle, the timings at which z_{cr} becomes shallower/deeper than the SML are similar to the values calculated by us. Since we cannot draw conclusion from the SML depth versus z_{cr} outside the autumn period we want to focus on Fig. 7b-c. During the first half of the autumn bloom period the SML is shallower than the critical depth ($\text{SML} < z_{cr}$) and surface Chl *a* concentrations increase (Fig. 7b-c). Throughout November the SML approaches z_{cr} . The SML is deeper than z_{cr} ($\text{SML} \geq z_{cr}$) from around mid November 2014 onwards, which coincides with depth integrated chlorophyll biomass (Fig. 6) and surface Chl *a* concentrations steadily decreasing to winter background levels of $< 1 \text{ mg m}^{-3}$ (Fig. 4c, Fig. 7c). This observed relationship does suggest that the SCD might be applicable to winter conditions and can be used to predict the shut-down of the autumn bloom, based on SML depth and surface irradiance values. Using these criteria to determine the shut-down of the autumn phytoplankton bloom we can estimate the bloom to have taken place between early October to November 20th 2014, which results in a duration of approximately 50 days.

4.3. Autumnal primary production

In order to assess the relative importance of primary production during the autumn bloom in comparison to the contribution to the

annual budget during the spring and summer months we make an estimate of new (gross) primary production based on the fraction of new nitrate supplied during the SML deepening that was taken up by phytoplankton.

Between summer and autumn the SML deepened from an average 21 m to 52 m (Fig. 5a, d). This would have entrained 31 m of bottom water with a nitrate concentration of $9.2 \pm 0.1 \mu\text{mol l}^{-1}$ (Fig. 5e). Distributing this over the 52 m autumn mixed layer gives a concentration of $5.5 \mu\text{mol l}^{-1}$. Knowing that in November only $2.1 \pm 0.1 \mu\text{mol l}^{-1}$ were observed in the surface layer (Fig. 4d, Fig. 5e), we assume that phytoplankton took up $3.4 \pm 0.1 \mu\text{mol l}^{-1}$ during the autumn bloom event. Using the elemental ratio of carbon (C) and nitrogen (N) found in phytoplankton we can convert the amount of utilised nitrate into an estimate of new, gross primary production. The C:N ratio of primary production has been shown to vary across a range of timescales, environmental conditions and between different phytoplankton groups (e.g. Geider and La Roche, 2002; Sterner, 2015; Moreno and Martiny, 2018). On average it tends to be close to the Redfield ratio, 106:16 (Redfield, 1934), which has more recently been revised to be 117:14 (Anderson and Sarmiento, 1994). Unfortunately, seasonally resolved observations of the C:N ratio were not available, but Humphreys et al. (2018) derived C:N ratios that span from spring - summer for each year of the SSB field campaign. For spring-summer 2014 Humphreys et al. (2018) found a C:N ratio of 117:13.0, which suggests a C rich production compared to Redfield. Observations by Davis et al. (2018) also suggest the production was C-rich compared to Redfield. They found that the composition of dissolved organic matter (DOM), which is a direct product of primary production, comprised $93 \pm 1\%$ of the total organic matter (TOM) during DY018 and, both pools, DOM and TOM, were reported to be C-rich compared to Redfield, with a C:N ratio of 12.5 ± 1.5 and 11.3 ± 1.2 , respectively (Davis et al., 2018). Throughout the observational campaign the C:N stoichiometry of the TOM pool showed little seasonal variability overall. The average ratios were comparable to previous studies in the Celtic Sea and other shelf seas that are characterised by nitrate limited production and thus the carbon and nitrate pools appeared to be closely coupled throughout (Davis et al., 2018 and references therein). In the

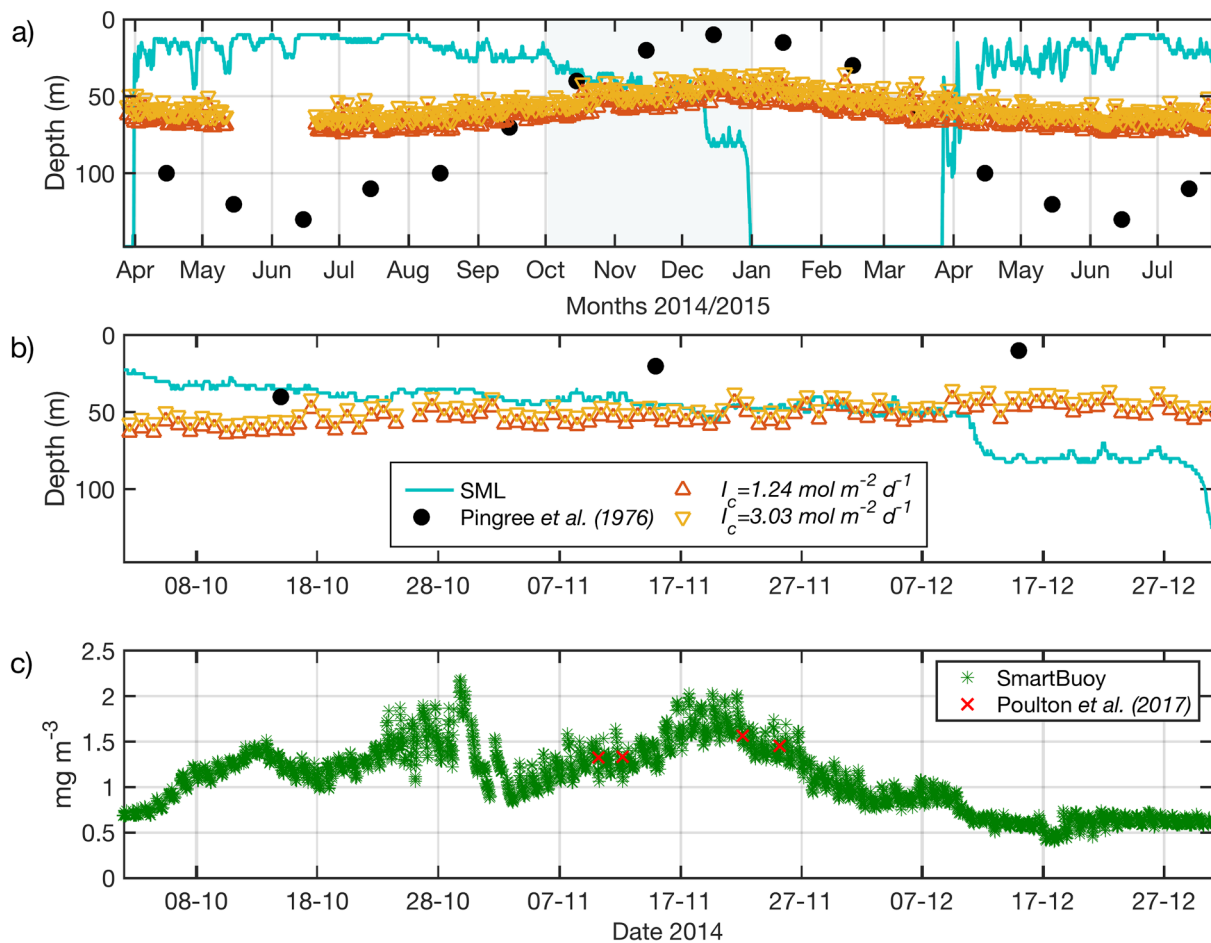


Fig. 7. Critical depth hypothesis. (a) Seasonal cycle of SML depth [m] (turquoise) compared to calculated values of z_{cr} using $I_c = 1.24 \text{ mol m}^{-2} \text{ d}^{-1}$ (orange), $I_c = 3.03 \text{ mol m}^{-2} \text{ d}^{-1}$ (yellow) and z_{cr} by Pingree et al. (1976) (black). The shaded area marks the time of active SML deepening (October 2nd - December 31st 2014). (b) same as (a) but focused on autumn period. (c) surface Chl *a* fluorescence [mg m^{-3}] observed by SmartBuoy (green) and CTD bottle samples (red) by Poulton et al. (2017) during autumn period. (For interpretation of the references to colour in this figure legend, the reader is referred to the web version of this article.)

absence of a cruise or season specific C:N ratio we thus assumed that the phytoplankton during autumn maintained the same C:N ratio as in spring and summer 2014 of 117:13.0 (Humphreys et al., 2018). In order to then derive the nitrate-supported C fixation we multiplied the converted amount of C by its molecular weight of 12 g mol^{-1} and obtained an estimate of $19.1 \pm 0.3 \text{ g C m}^{-2}$. Hence throughout a duration of 50 days, the autumn phytoplankton bloom potentially supported $382 \pm 6 \text{ mg C m}^{-2} \text{ d}^{-1}$ of new production.

In order to put the autumn phytoplankton bloom into context with other events during the seasonal cycle we calculated the equivalent new production rates for each season (Fig. 8). As before, we use the observed C:N ratios by Humphreys et al. (2018) who found C:N ratios of 117:13.0 and 117:12.2 for spring-summer 2014 and 2015, respectively.

For spring values we calculated new primary production rates based on the initial nitrate concentrations within the SML prior to the bloom and the average SML at the beginning of the bloom. The initial nitrate concentrations were simply defined as the pre-bloom concentrations of nitrate, these were $8 \pm 0.1 \mu\text{mol l}^{-1}$ in 2014 (DY008) and $7 \pm 0.1 \mu\text{mol l}^{-1}$ (DY021) in 2015 (Fig. 4d). Due to increased solar radiation and thus increased stratification the SML generally shoals throughout spring and summer (Fig. 2a-b). We therefore decided to use the average SML during the onset of the spring phytoplankton bloom in both years as this generally sets the depth over which nutrients will become depleted. Here we found average SML depths of 30 and 29 m for the spring period 2014 and 2015, respectively (Fig. 5b). The new (gross) primary production was then derived using the observed C:N ratios of 117:13.0 (Humphreys et al., 2018) as $25.9 \pm 0.1 \text{ g C m}^{-2}$ for

the spring phytoplankton bloom of 2014. While for the 2015 spring phytoplankton bloom we used the C:N ratio of 117:12.2 (Humphreys et al., 2018) and obtained an estimate of $23.4 \pm 0.3 \text{ g C m}^{-2}$. In order to obtain the daily production rates for each spring bloom event its duration had to be defined first. Using a 32 year-long record of monthly averaged data collected by a Continuous Plankton Recorder (CPR) at a shelf site in the Celtic Sea Joint et al. (2001) suggested a period of 2 months (April - May) for the spring phytoplankton bloom. This agrees well with our observations of overall increased surface Chl *a* concentrations during April-May 2014 and 2015 (Fig. 4c). It could be argued, that in 2014 the spring phytoplankton bloom actually concluded with the onset of the spring storm in late April 2014, which initiated a secondary peak in surface Chl *a* due to replenishment of surface nitrate (Fig. 2b, Fig. 4c and d). However we believe this is unlikely to occur every year and thus apply the commonly used duration of 60 days, which suggests rates of 432 ± 2 and $390 \pm 5 \text{ mg C m}^{-2} \text{ d}^{-1}$ of new production during spring 2014 and 2015, respectively.

During summer months surface nutrients are depleted (Fig. 4a) and hence new primary production within the SCM depend on diapycnal nutrient fluxes from the BML, which is the product of the vertical diffusivity at the base of the pycnocline, K_z [$\text{m}^2 \text{ s}^{-1}$], times the vertical nitrate gradient $\frac{\Delta N}{\Delta z}$ [mmol m^{-4}]. Here, ΔN is the difference in nitrate within the SML and BML, and Δz is the thickness of the nitracline. Due to the relatively low vertical resolution of discrete bottle samples, especially compared to physical data (Fig. 5a-c), deducing the thickness of the nitracline from discrete data points would have resulted in an underestimate of the nitrate gradient. Instead, we followed methods by

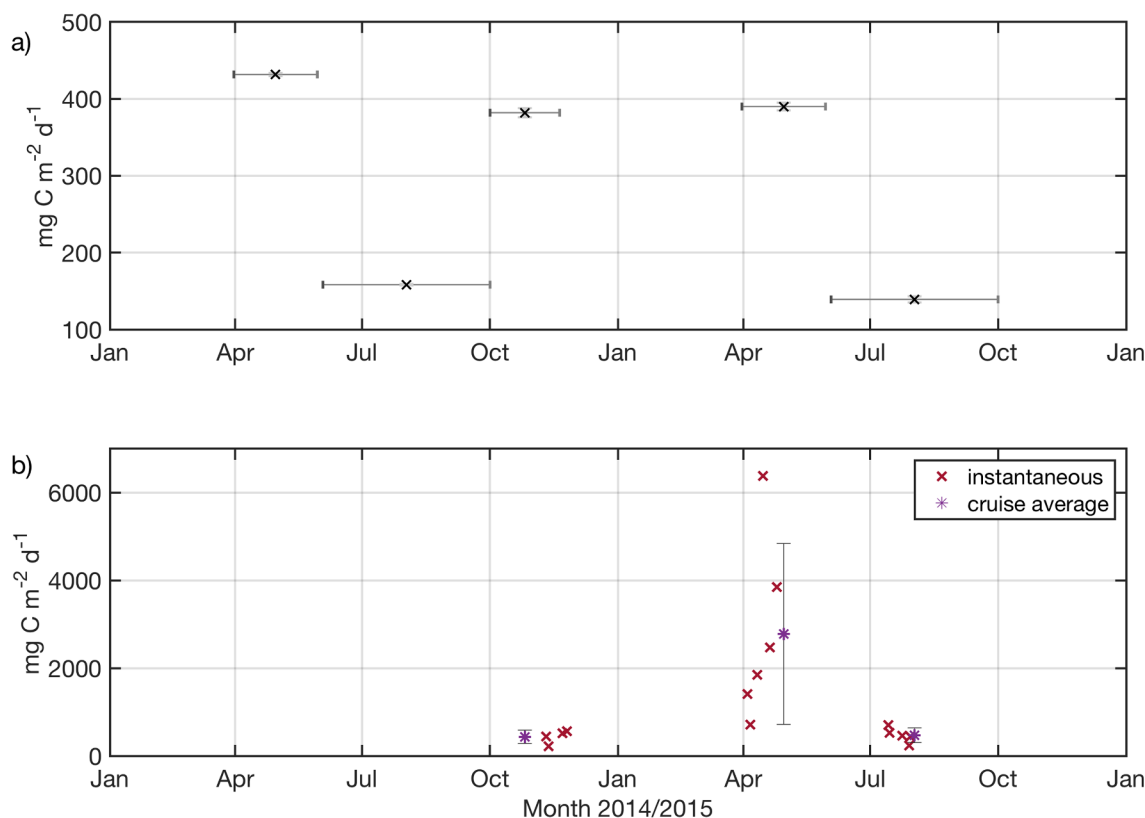


Fig. 8. Rates of primary production [$\text{mg C m}^{-2} \text{d}^{-1}$] at CCS. (a) gross (new) production, here horizontal bars show approximate duration of each seasonal state. (b) instantaneous (red crosses) and cruise averages (purple stars) of net primary production obtained by Poulton et al. (2017). Vertical bars in both panels denote error estimates (1 standard deviation). (For interpretation of the references to colour in this figure legend, the reader is referred to the web version of this article.)

Sharples et al. (2001), who defined the thickness of the nitracline between the depth of the SCM peak and the BML depth derived from CTD profiles. Using this method we found the nitracline thickness, Δz , to vary between 4.0 and 8.0 m during both DY026 (summer 2014) and DY033 (summer 2015). Using the average thickness of 5.5 m during DY026 resulted in a vertical nitrate gradient, $\frac{\Delta N}{\Delta z}$, of 1.7 mmol m^{-4} in summer 2014. Similarly, using the average thickness of 6.0 m during DY033 results in a vertical nitrate gradient of 1.4 mmol m^{-4} in summer 2015. By assuming a typical value for K_z (at the base of the pycnocline) of $1 \times 10^{-5} \text{ m}^2 \text{ s}^{-1}$ during both summers (Townsend, 1991; Benitez-Nelson et al., 2000; Sharples et al., 2001; Sharples et al., 2009) we obtained estimates of gross primary production rates of 158 ± 1 and $139 \pm 4 \text{ mg C m}^{-2} \text{ d}^{-1}$ in 2014 and 2015, respectively. As already mentioned by Townsend (1991), the amount of new production is extremely sensitive to the chosen value of K_z , and in reality the nitrate flux will vary with time in response to changes in tidal, wind and internal mixing (Sharples, 2008; Burchard and Rippeth, 2009; Williams et al., 2013). The current estimates are thus based on being supported by a background vertical flux of nitrate at the base of the thermocline. Our calculations thus do not reflect any short lived injections due to sporadic turbulent events and should be considered long-term estimates. Nevertheless, our rates for summer production agree with rates previously found in other temperate shelf seas (Townsend, 1991; Sharples et al., 2001; Williams et al., 2013).

By defining the summer regime as the period where new production is predominantly sustained by diapycnal nutrient fluxes, hence the time between spring bloom and autumnal deepening, suggests a duration of approximately 120 days (June - September), which is similar to previous estimates in temperate shelf seas (Hickman et al., 2012).

For ease of comparing our estimates of production rates among each other and with other studies, we summarised them in Table 3 & Fig. 8. The error bounds presented here take, where applicable, account of

Table 3

Carbon fixation rates (new production) [$\text{mg C m}^{-2} \text{d}^{-1}$] at CCS.

Season	Gross primary production [$\text{mg C m}^{-2} \text{d}^{-1}$]
Spring 2014	432 ± 2
Summer 2014	158 ± 1
Autumn 2014	382 ± 6
Spring 2015	390 ± 5
Summer 2015	139 ± 4

uncertainties (1 standard deviation) in the SML, BML & SCM depths as well as nitrate concentrations within the SML & BML.

Our results confirm the widely held view that the spring phytoplankton bloom is the dominant event fixing carbon in the seasonal cycle of primary production (e.g. Townsend et al., 1994; Rees et al., 1999; Sharples et al., 2006; Liu et al., 2010). The spring phytoplankton bloom in 2014 was characterised by the highest production rate of $432 \pm 2 \text{ mg C m}^{-2} \text{ d}^{-1}$ (Table 3 & Fig. 8a) within the observational period. During the observational campaign the production rates were lowest during the summer, sustaining 45 and 36% of the spring production in 2014 and 2015, respectively. The overall reduced production in 2015, compared to 2014, was potentially caused by a reduced nitrate inventory (Fig. 4d, Davis et al. (2018), Humphreys et al. (2018)) and overall weaker stratified conditions in summer 2015 compared to summer 2014 (Fig. 4a), which could result in a less effective diapycnal flux of nutrients into the euphotic layer during the summer months. We were surprised to see the rate of carbon production during autumn 2014 ($382 \pm 6 \text{ mg C m}^{-2} \text{ d}^{-1}$) was of similar magnitude to that of the following spring phytoplankton bloom 2015 ($390 \pm 5 \text{ mg C m}^{-2} \text{ d}^{-1}$), which suggests that the autumn phytoplankton bloom could act as a significant contributor to carbon fixation within the seasonal cycle.

Comparing our estimates to in situ measurements of net primary

productivity (NPP) at CCS by Poulton et al. (2017) shows some overlap in autumn 2014 (mean of $436 \text{ mg C m}^{-2} \text{ d}^{-1}$, range of $222\text{--}563 \text{ mg C m}^{-2} \text{ d}^{-1}$). Since our values (Table 3 & Fig. 8a) reflect the potential new production supported by the injection of new nitrate the relative agreement between our estimate and the NPP estimates by Poulton et al. (2017) suggests that a large fraction of the primary production during the autumn bloom was new rather than regenerated (approximately 88%). This is clearly higher than the estimated f -ratios proposed by Joint et al. (2001) that ranged between 0.25 and 0.39 throughout September and October using data sets obtained in the Celtic Sea. Joint et al. (2001) assumed f -ratios to increase during winter months to up to 0.5 during January and February. Taking an f -ratio of 0.4 and $382 \text{ mg C m}^{-2} \text{ d}^{-1}$ of new production suggests $955 \text{ mg C m}^{-2} \text{ d}^{-1}$ of total production, which is evidently higher than the maximum observed NPP rates found by Poulton et al. (2017). We do however note that 50% of the CCS samples by Poulton et al. (2017) were taken after our predicted shutdown of the autumn phytoplankton bloom due to insufficient light levels using the SCD hypothesis (Fig. 6 & Fig. 7c). While it is feasible that production still occurred, the decreasing trend in depth integrated chlorophyll biomass (Fig. 6) and surface Chl a (Fig. 7c) beyond this point suggests that production occurred at a reduced rate. These samples might therefore underrepresent the total production that took place during the autumn phytoplankton bloom.

Whilst assumptions we made about the bloom duration and the depth of the SML are justified based on the physical data presented here, we recognise that the C:N ratio of primary production is variable (eg Geider and La Roche, 2002; Sterner, 2015; Moreno and Martiny, 2018). Despite using the best available estimate of in situ C:N ratio at the time, we acknowledge the need for further research to better constrain the autumn phytoplankton bloom.

In addition to providing a third burst of primary production in the seasonal cycle of temperate shelves, the autumn phytoplankton bloom potentially plays a critical role in exporting carbon to the open ocean, which ultimately determines the efficiency of the continental shelf pump (Thomas et al., 2004; Chen and Borges, 2009; Barrón and Duarte, 2015). The autumn bloom is triggered by an increase in convection and wind mixing that gradually deepen the SML and ultimately restores a fully mixed water column. During the winter mixed period there is a weak net off-shelf transport (Ruiz-Castillo et al., 2018) that has the potential to remove organic material fixed on the outer shelf during the autumn bloom to deep water. During the spring and summer, when bottom water transport is more typically on-shelf (Ruiz-Castillo et al., 2018) removal of organic matter is less likely. The carbon fixed during the autumn bloom, just before the water column fully mixes may therefore constitute an important fraction of the carbon removed annually from the shelf.

5. Conclusion

This paper examined newly collected, long-term observational data of full-depth density, Chl a and nitrate profiles collected during the continuous 17 months observational campaign of the UK Shelf Sea Biogeochemistry programme. We observed an entire seasonal cycle of vertical density structure and its control on the seasonal cycle of primary productivity in a temperate shelf sea. The focus of this paper was the transition of vertical water column structure from summer to autumn, and its effect on the inorganic nutrients and chlorophyll biomass.

In an attempt to investigate the relative contributions to the vertical density structure from wind mixing, heating and convection, the Obukhov length scale (L_{OB} , Eq. (2)) was used, as it represents a balance between wind stress and buoyancy fluxes. The concept of Brody and Lozier (2014) provided a useful framework for this work (Table 2). Wind mixing (case 2 conditions) was shown to be the dominant control on density structure making the largest contribution for 53% of the time. This influence was found to further increase during October - December 2014 during the breakdown of stratification, wind being the

dominant control for 63% during this period. This is a potentially significant result since convection is typically thought to dominate SML deepening in autumn. We also observed that SML deepening during this period eroded an established SCM, whilst replenishing surface concentrations of nitrate. A subsequent increase in surface Chl a concentrations suggested in situ growth, which was confirmed by examining depth integrated chlorophyll biomass. The presence of detectable nitrate concentrations within the surface layer also suggested that primary production had shifted to become light limited. Building on the comprehensive understanding of water column dynamics and long-term time series of surface nitrate and Chl a we have investigated the role the autumn phytoplankton bloom plays within the seasonal cycle and estimated its contribution to annual primary production. We propose that the autumn bloom has the potential to act as a significant contributor to carbon fixation within the seasonal cycle. While the approach to winter appeared to have been a key time for shelf water to be exported into the NE Atlantic (Ruiz-Castillo et al., 2018), which could make the autumn productivity particularly important, further research is required to establish whether this may then contribute to the export of carbon into the deep ocean.

Acknowledgements

This work was funded by NERC and Defra as a part of the Shelf Sea Biogeochemistry strategic research programme, through the grants NE/K002007/1, NE/K002058/1, NE/K001701/1 and the Cefas grant NE/K001884/1. We thank the officers and crew of the RRS Discovery, RRS James Cook and RV Cefas Endeavour as well as staff at NMF-SS and NOC for their assistance in collecting the presented data sets. We thank Tom Bell (Plymouth Marine Laboratory) for sharing near surface thermistor data. We thank Jon Turton and the UK Met Office for supplying the Met Office ODAS Buoy and its data. The authors thank the NERC Earth Observation Data Acquisition and Analysis Service (NEODAAS) for supplying data for this study.

References

- Aiken, J., Fishwick, J., Moore, G., Pemberton, K., 2004. The annual cycle of phytoplankton photosynthetic quantum efficiency, pigment composition and optical properties in the western English Channel. *J. Marine Biological Assoc. U. K.* 84 (2), 301–313.
- Anderson, L.A., Sarmiento, J.L., 1994. Redfield ratios of remineralization determined by nutrient data analysis. *Global Biogeochem. Cycles* 8 (1), 65–80.
- Barrón, C., Duarte, C.M., 2015. Dissolved organic carbon pools and export from the coastal ocean. *Global Biogeochem. Cycles* 29 (10), 1725–1738.
- Bauer, J.E., Cai, W.-J., Raymond, P.A., Bianchi, T.S., Hopkinson, C.S., Regnier, P.A.G., 2013. The changing carbon cycle of the coastal ocean. *Nature* 504 (7478), 61–70.
- Behrenfeld, M.J., 2010. Abandoning Sverdrup's critical depth hypothesis on phytoplankton blooms. *Ecology* 91 (4), 977–989.
- Belcher, S.E., Grant, A.L.M., Hanley, K.E., Fox-Kemper, B., Van Roekel, L., Sullivan, P.P., ... Polton, J.A., 2012. A global perspective on Langmuir turbulence in the ocean surface boundary layer. *Geophys. Res. Lett.* 39 (18).
- Benitez-Nelson, C.R., Buesseler, K.O., Crossin, G., 2000. Upper ocean carbon export, horizontal transport, and vertical eddy diffusivity in the southwestern Gulf of Maine. *Cont. Shelf Res.* 20 (6), 707–736.
- Borges, A.V., Delille, B., Frankignoulle, M., 2005. Budgeting sinks and sources of CO_2 in the coastal ocean: diversity of ecosystems counts. *Geophys. Res. Lett.* 32 (14), 1–4.
- Brody, S.R., Lozier, M.S., 2014. Changes in dominant mixing length scales as a driver of subpolar phytoplankton bloom initiation in the North Atlantic. *Geophys. Res. Lett.* 41 (9), 3197–3203.
- Burchard, H., Rippeth, T.P., 2009. Generation of bulk shear spikes in shallow stratified tidal seas. *J. Phys. Oceanogr.* 39 (4), 969–985.
- Cai, W.-J., 2011. Estuarine and coastal ocean carbon paradox: CO_2 sinks or sites of terrestrial carbon incineration? *Ann. Rev. Marine Sci.* 3 (1), 123–145.
- Cai, W.-J., Dai, M., Wang, Y., 2006. Air-sea exchange of carbon dioxide in ocean margins: a province-based synthesis. *Geophys. Res. Lett.* 33 (12).
- Chen, C.-T.A., Borges, A.V., 2009. Reconciling opposing views on carbon cycling in the coastal ocean: continental shelves as sinks and near-shore ecosystems as sources of atmospheric CO_2 . *Deep Sea Res. Part II* 56 (8), 578–590.
- Chiswell, S.M., 2011. Annual cycles and spring blooms in phytoplankton: don't abandon Sverdrup completely. *Mar. Ecol. Prog. Ser.* 443, 39–50.
- Chiswell, S.M., Bradford-Grieve, J., Hadfield, M.G., Kennan, S.C., 2013. Climatology of surface chlorophyll a , autumn-winter and spring blooms in the southwest Pacific Ocean. *J. Geophys. Res.: Oceans* 118 (2), 1003–1018.

- Chiswell, S.M., Calil, P.H.R., Boyd, P.W., 2015. Spring blooms and annual cycles of phytoplankton: a unified perspective. *J. Plankton Res.* 37 (3), 500–508.
- Colebrook, J.M., Robinson, G.A., 1961. The seasonal cycle of the plankton in the North Sea and the north-eastern Atlantic. *J. Conseil* 26 (2), 156–165.
- Davis, C.E., Blackbird, S., Wolff, G., Woodward, M., Mahaffey, C., 2018. Seasonal organic matter dynamics in a temperate shelf sea. *Progr. Oceanography*. <https://doi.org/10.1016/j.pocean.2018.02.021>.
- Davis, C.E., Mahaffey, C., Wolff, G.A., Sharples, J., 2014. A storm in a shelf sea: variation in phosphorus distribution and organic matter stoichiometry. *Geophys. Res. Lett.* 41 (23), 8452–8459. [2014GL061949](https://doi.org/10.1029/2014GL061949).
- de Boyer Montégut, C., Madec, G., Fischer, A.S., Lazar, A., Iudicone, D., 2004. Mixed layer depth over the global ocean: an examination of profile data and a profile-based climatology. *J. Geophys. Res.: Oceans* 109 (C12), C12003.
- Dee, D.P., Uppala, S.M., Simmons, A.J., Berrisford, P., Poli, P., Kobayashi, S., ... Vitart, F., 2011. The ERA-Interim reanalysis: configuration and performance of the data assimilation system. *Q. J. R. Meteorological Soc.* 137 (656), 553–597.
- Du, C., Liu, Z., Kao, S.-J., Dai, M., 2017. Diapycnal fluxes of nutrients in an oligotrophic oceanic regime: the South China Sea. *Geophys. Res. Lett.* 44 (22), 11510–11518.
- Dugdale, R.C., Goering, J.J., 1967. Uptake of new and regenerated forms of nitrogen in primary productivity. *Limnol. Oceanogr.* 12 (2), 196–206.
- Dunne, J.P., Sarmiento, J.L., Gnanadesikan, A., 2007. A synthesis of global particle export from the surface ocean and cycling through the ocean interior and on the seafloor. *Global Biogeochem. Cycles* 21 (4), 1–16.
- Edinger, J.E., Duttweiler, D.W., Geyer, J.C., 1968. The response of water temperatures to meteorological conditions. *Water Resour. Res.* 4 (5), 1137–1143.
- Findlay, H.S., Yool, A., Nodale, M., Pitchford, J.W., 2006. Modelling of autumn plankton bloom dynamics. *J. Plankton Res.* 28 (2), 209–220.
- Franks, P.J.S., 2014. Has Sverdrup's critical depth hypothesis been tested? Mixed layers vs. turbulent layers. *ICES J. Marine Sci.: J. du Conseil* 72 (6), 1897–1907.
- García-Martín, E., Daniels, C.J., Davidson, K., Davis, C.E., Mahaffey, C., Mayers, K.M.J., McNeill, S., Poulton, A.J., Purdie, D.A., Tarran, G.A., Robinson, C., 2017. Seasonal changes in plankton respiration and bacterial metabolism in a temperate Shelf Sea. *Progr. Oceanography*. <https://doi.org/10.1016/j.pocean.2017.12.002>.
- Garrett, C.J.R., Keeley, J.R., Greenberg, D.A., 1978. Tidal mixing versus thermal stratification in the Bay of Fundy and Gulf of Maine. *Atmos. Ocean* 16 (4), 403–423.
- Geider, R.J., La Roche, J., 2002. Redfield revisited: variability of C:N:P in marine microalgae and its biochemical basis. *Eur. J. Phycol.* 37 (1), 1–17.
- Giering, S., Wells, S., Mayers, K., Schuster, H., Cornwell, L., Fileman, E., Atkinson, A., Cook, K., Preece, C., Mayor, D., 2018. Seasonal variation of zooplankton community structure and trophic position in the Celtic Sea: a stable isotope and biovolume spectrum approach. *Progr. Oceanography*. <https://doi.org/10.1016/j.pocean.2018.03.012>.
- Gill, A.E., 1982. *Atmosphere–Ocean Dynamics*. International Geophysics Series, vol. 30 Academic Press, New York.
- Gowen, R.J., Stewart, B.M., Mills, D.K., Elliott, P., 1995. Regional differences in stratification and its effect on phytoplankton production and biomass in the northwestern Irish Sea. *J. Plankton Res.* 17 (4), 753–769.
- Henson, S.A., Dunne, J.P., Sarmiento, J.L., 2009. Decadal variability in North Atlantic phytoplankton blooms. *J. Geophys. Res.: Oceans* 114 (C4).
- Hickman, A.E., Moore, C.M., Sharples, J., Lucas, M.I., Tilstone, G.H., Krivtsov, V., Holligan, P.M., 2012. Primary production and nitrate uptake within the seasonal thermocline of a stratified shelf sea. *Mar. Ecol. Prog. Ser.* 463, 39–57.
- Holt, J., Icarus, J.A., Anderson, T.R., Brewin, R., Butenschön, M., Harle, J., Huse, G., Lehodey, P., Lindemann, C., Memery, L., Salihoglu, B., Senina, I., Yool, A., 2014. Challenges in integrative approaches to modelling the marine ecosystems of the North Atlantic: physics to fish and coasts to ocean. *Progr. Oceanography* 129 (Part B), 285–313.
- Hopkins, J.E., Stephenson, G.R., Green, J.M., Inall, M.E., Palmer, M.R., 2014. Storms modify baroclinic energy fluxes in a seasonally stratified shelf sea: Inertial-tidal interaction. *J. Geophys. Res.: Oceans* 119 (10), 6863–6883.
- Hu, S., Chen, C., Ji, R., Townsend, D.W., Tian, R., Beardsley, R.C., Davis, C.S., 2011. Effects of surface forcing on interannual variability of the fall phytoplankton bloom in the Gulf of Maine revealed using a process-oriented model. *Mar. Ecol. Prog. Ser.* 427, 29–49.
- Hull, T., Greenwood, N., Kaiser, J., Johnson, M., 2016. Uncertainty and sensitivity in optode-based shelf-sea net community production estimates. *Biogeosciences* 13 (4), 943–959.
- Humphreys, M.P., Achterberg, E.P., Hopkins, J.E., Chowdhury, M.Z.H., Griffiths, A.M., Hartman, S.E., Hull, T., Smilenova, A., Wihsott, J.U., Woodward, E.M.S., Moore, C.M., 2018. Mechanisms for a nutrient-conserving carbon pump in a seasonally stratified, temperate continental shelf sea. *Progr. Oceanography*. <https://doi.org/10.1016/j.pocean.2018.05.001>.
- Hydes, D.J., Aoyama, M., Aminot, A., Bakker, K., Becker, S., Coverly, S., Daniel, A., Dickson, A., Grosso, O., Kerouel, R., Van Ooijen, J., Sato, K., Tanhua, T., Woodward, E.M.S., Zhang, J., 2010. Determination of dissolved nutrients (N, P, Si) in seawater with high precision and inter-comparability using gas-segmented continuous flow analysers. In: *The GO-SHIP Repeat Hydrography Manual: A Collection of Expert Reports and guidelines*. IOCCP Report No 14, ICPO Publication Series No. 134, version 1. 2010 (UNESCO/IOC).
- Ji, R., Davis, C.S., Chen, C., Townsend, D.W., Mountain, D.G., Beardsley, R.C., 2008. Modeling the influence of low-salinity water inflow on winter-spring phytoplankton dynamics in the Nova Scotian Shelf-Gulf of Maine region. *J. Plankton Res.* 30 (12), 1399–1416.
- Joint, I., Wollast, R., Chou, L., Batten, S., Elskens, M., Edwards, E., ... Woolfenden, J., 2001. Pelagic production at the Celtic Sea shelf break. *Deep Sea Res. Part II* 48 (14–15), 3049–3081.
- Kirkwood, D., 1996. *Nutrients: Practical notes on their determination in sea water*. Number 17. International Council for the Exploration of the Sea.
- Kraus, E.B., Turner, J.S., 1967. A one-dimensional model of the seasonal thermocline II. The general theory and its consequences. *Tellus* 19 (1), 98–106.
- Kröger, S., Parker, E.R., Metcalfe, J.D., Greenwood, N., Forster, R.M., Sivyer, D.B., Pearce, D.J., 2009. Sensors for observing ecosystem status. *Ocean Sci.* 5 (4), 523–535.
- Lacombe, H., Tchernia, P., Charcot, J., Ribet, M., Bonnot, J., Frassetto, R., Swallow, J.C., 1970. Observation of formation of deep water in the Mediterranean Sea, 1969. *Nature* 227, 1037–1040.
- Landry, M.R., Hassett, R.P., 1982. Estimating the Grazing Impact of Marine Micro-zooplankton. *Mar. Biol.* 67 (3), 283–288.
- Langdon, C., 1988. On the causes of interspecific differences in the growth-irradiance relationship for phytoplankton. II. A general review. *J. Plankton Res.* 10 (6), 1291–1312.
- Lee, K., Matsuno, T., Endoh, T., Ishizaka, J., Zhu, Y., Takeda, S., Sukigara, C., 2016. A role of vertical mixing on nutrient supply into the subsurface chlorophyll maximum in the shelf region of the East China Sea. *Cont. Shelf Res.* 143, 139–150.
- Liu, K.-K., 2010. *Biogeochemistry of Continental Margins in a Global Context*. In: K.-K. Liu, L. Atkinson, R. Quiñones, and L. Talaeu-McManus (Eds.), *Carbon and nutrient fluxes in continental margins: a global synthesis*, IGBP Book Series, vol. 3–24. Berlin: Springer Science & Business Media, Chapter 1, 741.
- Longhurst, A., 1995. Seasonal cycles of pelagic production and consumption. *Progr. Oceanogr.* 36 (2), 77–167.
- Marshall, J., Schott, F., 1999. Openocean convection: observations, theory, and models. *Rev. Geophys.* 37 (1), 1–64.
- Martinez, E., Antoine, D., D'Ortenzio, F., De Boyer Montégut, C., 2011. Phytoplankton spring and fall blooms in the North Atlantic in the 1980s and 2000s. *J. Geophys. Res.: Oceans* 116 (C11), 1–11.
- McDougall, T.J., Barker, P.M., 2011. *Getting started with TEOS-10 and the Gibbs Seawater (GSW) Oceanographic Toolbox*. SCOR/IAPSO WG, 127, 1–28. ISBN 978-0-646-55621-5.
- Moreno, A.R., Martiny, A.C., 2018. Ecological stoichiometry of ocean plankton. *Ann. Rev. Marine Sci.* 10 (1), 43–69.
- Muller-Karger, F.E., Varela, R., Thunell, R., Luerssen, R., Hu, C., Walsh, J.J., 2005. The importance of continental margins in the global carbon cycle. *Geophys. Res. Lett.* 32 (1), L01602.
- Nielsen, M.H., St. John, M., 2001. Modelling thermal stratification in the North Sea: application of a 2-D potential energy model. *Estuar. Coast. Shelf Sci.* 53 (5), 607–617.
- Obukhov, A.M., 1946. *Turbulentnost' v temperaturnoje neodnorodnoj atmosfere* (Turbulence in an Atmosphere with a Non-uniform Temperature). Trudy Inst. Theor. Geofiz. AN SSSR 1, 95–115.
- Pemberton, K., Rees, A.P., Raine, R., Joint, I., 2004. The influence of water body characteristics on phytoplankton diversity and production in the Celtic Sea. *Cont. Shelf Res.* 24 (17), 2011–2028.
- Pingree, R.D., Griffiths, D.K., 1977. The bottom mixed layer on the continental shelf. *Estuar. Coast. Mar. Sci.* 5 (3), 399–413.
- Pingree, R.D., Holligan, P.M., Mardell, G.T., Head, R.N., 1976. The influence of physical stability on spring, summer and autumn phytoplankton blooms in the Celtic Sea. *J. Marine Biological Assoc. U. K.* 56 (04), 845–873.
- Pingree, R.D., Mardell, G.T., Holligan, P.M., Griffiths, D.K., Smithers, J., 1982. Celtic Sea and Armorican current structure and the vertical distributions of temperature and chlorophyll. *Cont. Shelf Res.* 1 (1), 99–116.
- Poulton, A.J., Davis, C.E., Daniels, C.J., Mayers, K.M.J., Harris, C., Tarran, G.A., Widdicombe, C.E., Woodward, E.M.S., 2017. Seasonal phosphorus and carbon dynamics in a temperate shelf sea (Celtic Sea). *Progr. Oceanography*. <https://doi.org/10.1016/j.pocean.2017.11.001>.
- Redfield, A.C., 1934. On the proportions of organic derivatives in sea water and their relation to the composition of plankton. James Johnstone Memorial Volume. University Press of Liverpool.
- Rees, A.P., Joint, I., Donald, K.M., 1999. Early spring bloom phytoplankton-nutrient dynamics at the Celtic Sea Shelf Edge. *Deep Sea Res. Part I* 46 (3), 483–510.
- Regnier, P., Friedlingstein, P., Ciais, P., Mackenzie, F.T., Gruber, N., Janssens, I.A., ... Thullner, M., 2013. Anthropogenic perturbation of the carbon fluxes from land to ocean. *Nature Geosci.* 6 (8), 597–607.
- Ruiz-Castillo, E., Sharples, J., Hopkins, J., Woodward, M., 2018. Seasonality in the cross-shelf physical structure of a temperate shelf sea and the implications for nitrate supply. *Progr. Oceanography*. <https://doi.org/10.1016/j.pocean.2018.07.006>.
- Seguro, I., Marca, A.D., Painting, S.J., Shutler, J.D., Suggett, D.J., Kaiser, J., 2017. High-resolution net and gross biological production during a Celtic Sea spring bloom. *Progr. Oceanography*. <https://doi.org/10.1016/j.pocean.2017.12.003>.
- Sharples, J., 1999. Investigating the seasonal vertical structure of phytoplankton in shelf seas. *Marine Models* 1 (1–4), 3–38.
- Sharples, J., 2008. Potential impacts of the spring-neap tidal cycle on shelf sea primary production. *J. Plankton Res.* 30 (2), 183–197.
- Sharples, J., Ellis, J.R., Nolan, G., Scott, B.E., 2013. Fishing and the oceanography of a stratified shelf sea. *Progr. Oceanogr.* 117 (0), 130–139.
- Sharples, J., Moore, C.M., Hickman, A.E., Holligan, P.M., Tweddle, J.F., Palmer, M.R., Simpson, J.H., 2009. Internal tidal mixing as a control on continental margin ecosystems. *Geophys. Res. Lett.* 36 (23), L23603.
- Sharples, J., Moore, M.C., Rippeth, T.P., Holligan, P.M., Hydes, D.J., Fisher, N.R., Simpson, J.H., 2001. Phytoplankton distribution and survival in the thermocline. *Limnol. Oceanogr.* 46 (3), 486–496.
- Sharples, J., Poulton, A.J., Rees, A., Robinson, C., this issue. Preface: The UK Shelf Sea Biogeochemistry Research programme - Seasonality in biogeochemical processes over a stratifying shelf sea. *Progr. Oceanography*.
- Sharples, J., Ross, O.N., Scott, B.E., Greenstreet, S.P.R., Fraser, H., 2006. Inter-annual

- variability in the timing of stratification and the spring bloom in the North-western North Sea. *Cont. Shelf Res.* 26 (6), 733–751.
- Siegel, D.A., Doney, S.C., Yoder, J.A., 2002. The North Atlantic Spring Phytoplankton Bloom and Sverdrup's Critical Depth Hypothesis. *Science* 296 (5568), 730.
- Simpson, J.H., Bowers, D.G., 1984. The role of tidal stirring in controlling the seasonal heat cycle in shelf seas. *Ann. Geophys.* 2 (4), 411–416.
- Simpson, J.H., Hunter, J.R., 1974. Fronts in the Irish Sea. *Nature* 250, 404–406.
- Smayda, T.J., 1957. Phytoplankton studies in lower Narragansett Bay. *Limnol. Oceanogr.* 2 (4), 342–359.
- Song, H., Ji, R., Stock, C., Kearney, K., Wang, Z., 2011. Interannual variability in phytoplankton blooms and plankton productivity over the Nova Scotian Shelf and in the Gulf of Maine. *Mar. Ecol. Prog. Ser.* 426, 105–118.
- Song, H., Ji, R., Stock, C., Wang, Z., 2010. Phenology of phytoplankton blooms in the Nova Scotian Shelf–Gulf of Maine region: remote sensing and modeling analysis. *J. Plankton Res.* 32 (11), 1485–1499.
- Sterner, R.W., 2015. Ocean stoichiometry, global carbon, and climate. *Proc. Nat. Acad. Sci.* 112 (27), 8162–8163.
- Sverdrup, H.U., 1953. On conditions for the vernal blooming of phytoplankton. *J. Conseil* 18 (3), 287–295.
- Taylor, J.R., Ferrari, R., 2011. Shutdown of turbulent convection as a new criterion for the onset of spring phytoplankton blooms. *Limnol. Oceanogr.* 56 (6), 2293–2307.
- Tett, P.B., Joint, I.R., Purdie, D.A., Baars, M., Oosterhuis, S., Daneri, G., ... Lankester, R., 1993. Biological Consequences of Tidal Stirring Gradients in the North Sea [and Discussion]. *Philos. Trans. R. Soc. London. Ser. A: Phys. Eng. Sci.* 343 (1669), 493.
- Thomas, A.C., Townsend, D.W., Weatherbee, R., 2003. Satellite-measured phytoplankton variability in the Gulf of Maine. *Cont. Shelf Res.* 23 (10), 971–989.
- Thomas, H., Bozec, Y., Elkalay, K., De Baar, H.J.W., 2004. Enhanced open ocean storage of CO₂ from shelf sea pumping. *Science* 304 (5673), 1005–1008.
- Townsend, D.W., 1991. Influences of oceanographic processes on the biological productivity of the Gulf of Maine. *Rev. Aquat. Sci.* 5 (3), 211–230.
- Townsend, D.W., Cammen, L.M., Holligan, P.M., Campbell, D.E., Pettigrew, N.R., 1994. Causes and consequences of variability in the timing of spring phytoplankton blooms. *Deep Sea Res. Part I* 41 (5), 747–765.
- Townsend, D.W., Pettigrew, N.R., Thomas, M.A., Neary, M.G., McGillicuddy, J., Dennis, J., O'Donnell, J., 2015. Water masses and nutrient sources to the Gulf of Maine. *J. Mar. Res.* 73 (3–4), 93–122.
- Townsend, D.W., Rebuck, N.D., Thomas, M.A., Karp-Boss, L., Gettings, R.M., 2010. A changing nutrient regime in the Gulf of Maine. *Cont. Shelf Res.* 30 (7), 820–832.
- Wihsgott, J.U., Hopkins, J.E., Sharples, J., Jones, E., Balfour, C., 2016. Long-term mooring observations of full depth water column structure spanning 17 months, collected in a temperate shelf sea (Celtic Sea). https://www.bodc.ac.uk/data/published_data_library/catalogue/10.5285/389fe406-ebd9-74f1-e053-6c86abc032a4/. Available from British Oceanographic Data Centre, Natural Environment Research Council.
- Wihsgott, J.U., Hopkins, J.E., Sharples, J., Jones, E., Balfour, C., 2018. Long-term, full depth observations of horizontal velocities spanning 17 months, collected in a temperate shelf sea (Celtic Sea) on the NW European Shelf. <https://dx.doi.org/10.5285/631ddd2a-48df-143b-e053-6c86abc0d49f>. Available from British Oceanographic Data Centre, Natural Environment Research Council.
- Williams, C., Sharples, J., Green, M., Mahaffey, C., Rippeth, T., 2013. The maintenance of the subsurface chlorophyll maximum in the stratified western Irish Sea. *Limnol. Oceanogr.: Fluids Environ.* 3 (1), 61–73.
- Williams, C., Sharples, J., Mahaffey, C., Rippeth, T., 2013. Wind-driven nutrient pulses to the subsurface chlorophyll maximum in seasonally stratified shelf seas. *Geophys. Res. Lett.* 40 (20), 5467–5472.
- Wollast, R., 1998. Evaluation and comparison of the global carbon cycle in the coastal zone and in the open ocean. In: In: Brink, K.H., Robinson, A.R. (Eds.), *The Sea*, vol. 10. John Wiley & Sons Inc., pp. 213–252 (Chapter 9).
- Woodward, E.M.S., Rees, A.P., 2001. Nutrient distributions in an anticyclonic eddy in the northeast Atlantic Ocean, with reference to nanomolar ammonium concentrations. *Deep Sea Res. Part II* 48 (4), 775–793.